IEEE Access
Multidisciplinary | Rapid Review | Open Access Journal

Received September 26, 2019, accepted October 6, 2019, date of publication October 15, 2019, date of current version October 29, 2019.

Digital Object Identifier 10.1109/ACCESS.2019.2947497

Target Localization in Multipath Propagation Environment Using Dictionary-Based Sparse Representation

YUAN LIU[1], HONGWEI LIU[2], (Member, IEEE), XIANG-GEN XIA[3,4], (Fellow, IEEE), LU WANG[1], AND GUOAN BI[1], (Senior Member, IEEE)

[1]School of Electrical and Electronic Engineering, Nanyang Technological University, Singapore 639798
[2]National Laboratory of Radar Signal Processing, Xidian University, Xi'an 710071, China
[3]College of Telecommunications Engineering, Xidian University, Xi'an 710071, China
[4]Department of Electrical and Computer Engineering, University of Delaware, Newark, DE 19716, USA

Corresponding authors: Hongwei Liu (hwliu@xidian.edu.cn) and Guoan Bi (egbi@ntu.edu.sg)

This work was supported by the National Science Fund for Distinguished Young Scholars under Grant 61525105.

ABSTRACT This paper addresses the target localization problem in complex multipath propagation environment for three-dimensional (3-D) radar systems. Firstly, an approach based on the singular value decomposition (SVD) technique is developed to reduce the data dimension and formulate the joint multiple snapshot sparse representation problem in the signal subspace domain. Subsequently, a novel sparse representation based DOA estimation algorithm, combined with alternatingly iterative and dictionary refinement techniques, is proposed. The Cramér-Rao bounds (CRB) for the target DOA and attenuation coefficient estimations of multipath model are derived in closed forms. Experimental results based on both simulated data and measured data indicate that the target localization accuracy can be effectively enhanced by utilizing the proposed algorithm in complex terrain and/or limited snapshot scenarios.

INDEX TERMS Cramér-Rao bound (CRB), direction of arrival (DOA) estimation, parameterized dictionary refinement, multipath propagation, sparse representation.

I. INTRODUCTION

It is well-known that one of the critical missions achieved by modern three-dimensional (3-D) radar is measuring the altitude of a target. However, when tracking a low-angle target, the localization performance of radar system may be affected by the multipath phenomenon from ground surface reflection, i.e., target echoes consisting of a direct path as well as highly correlated multipath [1]–[4]. Because the target and multipath signals are within the same beamwidth, it is difficult to separate them in the spatial, time, and/or Doppler domains. There have been considerable efforts to deal with this problem in the conventional radar systems since 1970s, for example, [1]–[11].

The key issue of target altitude measurement is to estimate its DOA from the radar echo corrupted by the multipath propagation. The most well-known existing nonparametric DOA estimation methods include subspace-based methods [5]–[8] and digital beamforming (DBF) [9]. Beamforming spectrum is limited by the Rayleigh resolution boundary. Although the popular subspace-based methods, such as multiple signal classification (MUSIC) [5], can be modified to be used in multipath scenario by applying the spatial smoothing technique [6], the decorrelation preprocessing may reduce the effective array aperture and result in radar performance degradation. To address this problem, an improved target localization algorithm based on eigen-decomposition and alternating projection is presented in our previous work [12]. It is shown that the spatial smoothing preprocessing can be avoided by introducing a composite steering vector that contains the coherent structure information of the spatial signals and the target localization performance can be improved by exploiting the multipath structure information. However, it is worth mentioning that most of the subspace-based methods (including the method in [12]) depend on the asymptotic assumptions (e.g., requiring a sufficient number of snapshots). Nevertheless, due to some unsolvable restrictions in practical applications, e.g., limited observation time and/or

The associate editor coordinating the review of this manuscript and approving it for publication was Chengpeng Hao.

complex background environment, only a very limited number of snapshots or, even in the worst case, a single time sample is available. For example, our previous work [13] shows that only one snapshot can be available in some coherent processing intervals (CPIs) of the real measured data. Under the condition mentioned above, the performance of these algorithms that rely on the estimates of the sample covariance matrix is degraded significantly or even fail to work since it is rank deficient [7], [14]. Another family of parametric techniques [15]–[22] mainly based on the maximum likelihood (ML) paradigm, including the relax algorithm [15], the alternation projection maximum likelihood (AP-ML) algorithm [19] and the refined maximum likelihood (RML) algorithms [20]–[22], which enjoy excellent statistical properties, can be applied in the coherent signal scenario.

In the above-mentioned target localization methods, the multipath propagation is usually studied with the implicit assumption that the highly deterministic multipath signal model holds, or in other words, the geometry relationship between the target and image signals is fixed. However, the geometry relationship may be time-varying, which is very difficult to be determined in practice since the Earth's surface is spatially variant [23], [24]. The detailed explanation can also be found in [25], where the target direction is obtained by using the technique of rank-one constraint and CS theory in a MIMO radar system. Thus, the existing highly deterministic multipath signal model based target localization algorithms may become invalid for a complex terrain. Considering the sufficient sparsity of the signals in the elevation direction, sparse signal representation technique can be applied to the problem of low-angle target localization, which is the main interest of this paper. The sparsity of spatial signals can be reduced to be one by introducing a parametric adaptive dictionary and the inner structure of the dictionary can be enhanced by taking the multipath attenuation coefficient into account, both of which are not considered in [25]. By focusing on the sparse signal representation framework, super-resolution can be achieved with lower sensitivity to the correlation of the signals and without the need to use a large number of snapshots.

The main contributions of this paper are summarized as follows:

1) A new adaptation of sparse signal representation to target localization in the presence of multipath propagation is presented. By introducing a parametric adaptive dictionary, the inner structure information of the target and its multipath image can be sufficiently exploited and the sparsity of spatial signals is reduced to be one. Compared with the existing highly deterministic multipath signal model based algorithms, the proposed algorithm can deal with the effect of multipath phenomenon from both simple and complex terrains with a limited number of time samples and without the need of any prior knowledge on the spatial distribution of multipath.
2) The preprocessing step by using singular value decomposition (SVD) technique is introduced to enhance the signal to noise ratio (SNR) and to formulate the target localization problem with multiple snapshots in the signal subspace domain so that the proposed approach can be used for real-time application.
3) Alternatingly iterative scheme and adaptive dictionary refinement techniques are introduced to deal with the resulting objective function optimization problem and to reduce the computational cost, in which the target localization and the parameterized dictionary refinement can be adaptively realized.
4) The CRB for the estimation is derived. In our Monte-Carlo simulations and real data analysis, the proposed algorithm performs with some advantages over the other existing state-of-the-art algorithms, i.e., it has increased accuracy of target localization and improved performance robustness with a limited number of snapshots.

A preliminary and short version of this paper was presented as a conference paper at CoSeRa [13]. This elaborated version includes detailed clarification of our previous results, and also the derivation of the CRB and more analysis on experimental results from simulated and real data.

The remainder of this paper is organized as follows. A brief introduction to the practical multipath signal model for low-angle target localization is given in Section II. In Section III, the proposed algorithm is presented in detail. Experimental results based on simulation data and measured data as well as the comparison to some other methods are discussed in Section IV. Finally, the conclusion of this paper is drawn in Section V.

Notations: Matrices, vectors and scalar quantities are written in bold upper-case, bold lower-case and normal letters, respectively. The notations $(\cdot)^T$, $(\cdot)^H$, $(\cdot)^*$, $|\cdot|$, $tr\{\cdot\}$, $E\{\cdot\}$ and $(\cdot)^{-1}$ represent operations of transpose, conjugate transpose, complex conjugate, absolute value, trace, expectation and inverse, respectively. The notations $\|\cdot\|_F$, $\|\cdot\|_*$, $\odot$, $\mathrm{Re}\{\cdot\}$ and $\mathbb{C}^{M\times N}$ denote Frobenius norm, nuclear norm, Hadamard product, real part extraction and $M \times N$ complex matrix, respectively.

II. PROBLEM FORMULATION

Consider an array radar system containing M omni-directional sensors. A simple illustration of the multipath propagation geometry is depicted in Fig. 1. There are two separate paths between the target T and the radar A, the direct path (AT) with elevation θ_d and the indirect path (ABT), via reflection with grazing angle ψ_g from the ground surface, which has an elevation angle θ_s, where Point B is the gradient ground reflection point. The dotted line (ACT) shows the conventional multipath model that is reflected by a perfectly smooth surface. h_a, h_t and h_g are the heights of the array antenna center, the target and the reflection point, respectively. R_d and R_s are the distance between radar and target and the distance between radar and image, respectively.

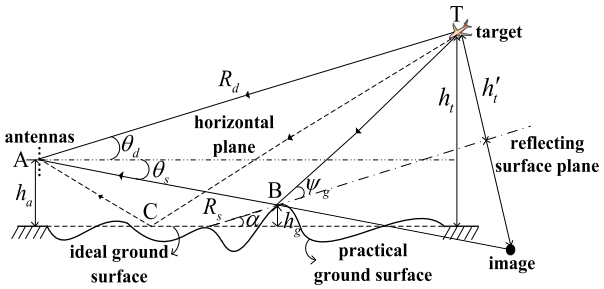

FIGURE 1. Multipath propagation geometry in complex terrain environment, where the dashed line, the dash-dotted line and the double dot dashed line represent the conventional propagation model in an ideal smooth ground surface, the reflecting surface plane and the horizontal plane, respectively.

The vertical distance from the target to the reflecting surface and the included angle between the reflecting surface and the ideal smooth surface are h_t' and α, respectively.

A. RECEIVED SIGNAL MODEL

Suppose the emitted signal $u(t)$ is a narrow-band signal, expressed as

$$u(t) = s(t)\exp\left(j\left(2\pi f_0 t + \phi_0\right)\right) \tag{1}$$

where $s(t)$ is the baseband signal, f_0 and ϕ_0 are the carrier frequency and the initial phase, respectively. For convenience and without loss of generality, ϕ_0 is assumed to be zero. The target is located at such a distance that the arriving waves can be considered as being planar, as shown in Fig. 1. The output of the mth sensor can be expressed as

$$\begin{aligned} s_{r,m}(t) &= a\left(u\left(t-\tau_{d,m}\right) + \rho u\left(t-\tau_{s,m}\right)\right) + n_m(t) \\ &= ae^{j2\pi f_0 t}\begin{pmatrix} s\left(t-\tau_{d,m}\right)e^{-j2\pi f_0\tau_{d,m}} \\ +\rho s\left(t-\tau_{s,m}\right)e^{-j2\pi f_0\tau_{s,m}} \end{pmatrix} + n_m(t) \end{aligned} \tag{2}$$

where a is the target reflection coefficient, ρ is the specular reflection coefficient, $n_m(t)$ is the additive Gaussian white noise of the mth sensor with zero mean and variance σ_N^2. $\tau_{d,m}$ and $\tau_{s,m}$ are the time delays of the direct path and the multipath for the mth sensor, respectively. $\tau_{d,m}$ and $\tau_{s,m}$ can be further expressed as

$$\tau_{d,m} = \tau_0 + \tau_m(\theta_d) \tag{3}$$

$$\tau_{s,m} = \tau_0 + \Delta\tau + \tau_m(\theta_s) \tag{4}$$

where τ_0 and $\Delta\tau$ are the time delay from the target to the referenced sensor and the delay difference between the direct path and the multipath, respectively. $\tau_m(\theta_d)$ and $\tau_m(\theta_s)$ are the relative delays between the mth sensor and the referenced sensor at directions θ_d and θ_s, respectively.

Because the received waveform is narrow-band, the time delay within the term of baseband signal in (2) can be ignored. Thus, we have the following representation

$$s\left(t-\tau_{d,m}\right) \approx s\left(t-\tau_{s,m}\right) \approx s\left(t-\tau_0\right). \tag{5}$$

Substituting (3), (4) and (5) into (2), (6) can be simply derived as

$$s_r(t) = ae^{j(2\pi f_0(t-\tau_0))}\begin{pmatrix} e^{-j2\pi f_0\tau_m(\theta_d)} \\ +\bar{\rho}e^{-j2\pi f_0\tau_m(\theta_s)} \end{pmatrix} s\left(t-\tau_0\right) + n_m(t) \tag{6}$$

where $\bar{\rho} = \rho e^{-j2\pi\Delta R/\lambda}$ is the multipath attenuation coefficient. $\Delta R = R_s - R_d$ and λ are the path difference and the wavelength, respectively. By measuring the time relative to the referenced phase center, the dependence on τ_0 can be dropped. After demodulation, the final matrix-vector version of the basic narrow-band observation in (6) takes the following form:

$$\mathbf{x}(t) = a\left[\mathbf{a}(\theta_d), \mathbf{a}(\theta_s)\right]\left[1, \bar{\rho}\right]^T s(t) + \mathbf{n}(t) \tag{7}$$

where $\mathbf{a}(\theta_d)$ and $\mathbf{a}(\theta_s)$ are the so-called steering vectors of the array toward directions of the target and its image, respectively. $\mathbf{n}(t) = [n_1(t), \cdots, n_m(t), \cdots, n_M(t)]^T$, $t = t_1, \cdots, t_L$ where L is the number of snapshots in a coherent processing interval (CPI). It is worth mentioning that a is equal to zero when there is no target in the scene. Given the knowledge of $\mathbf{x}(t)$, the goal is to find the unknown location of the target, i.e., θ_d in (7).

B. MULTIPATH REFLECTION COEFFICIENT ANALYSIS

The specular reflection coefficient ρ, given in (2), is defined as the ratio of the electric field phasor of the image signal over that of the target signal. Some detailed explanation of ρ can be found in [26]. Generally, ρ can be represented as

$$\rho = \rho_\Gamma \rho_D \rho_s \tag{8}$$

where ρ_Γ, ρ_D and ρ_s represent the Fresnel reflection coefficient, the divergence factor and the specular scattering factor, respectively. The expressions of ρ_Γ for vertical and horizontal polarizations were derived in [27], respectively expressed as

$$\rho_{\Gamma v} = \frac{\varepsilon_c \sin\psi_g - \sqrt{\varepsilon_c - \cos^2\psi_g}}{\varepsilon_c \sin\psi_g + \sqrt{\varepsilon_c - \cos^2\psi_g}} \tag{9}$$

and

$$\rho_{\Gamma h} = \frac{\sin\psi_g - \sqrt{\varepsilon_c - \cos^2\psi_g}}{\sin\psi_g + \sqrt{\varepsilon_c - \cos^2\psi_g}} \tag{10}$$

where ε_c is the complex dielectric constant, expressed as

$$\varepsilon_c = \varepsilon_r - j\lambda\delta\big/2\pi c\varepsilon_0 \tag{11}$$

where ε_r and δ are the relative dielectric constant and the conductivity, respectively. c is the speed of light, $\varepsilon_0 = 8.85 \times 10^{-12}$ F/m and the unit F/m is Farad per meter. ρ_D is introduced due to the spherical surface of the Earth, and the detailed description of ρ_D can be referred to [28] and [29]. Another factor ρ_s is used to describe the reduction of the magnitude of the specular reflection coefficient, which is

caused by the randomness of the terrain. A simple model of ρ_s was reported in [30] and [31], given as

$$\rho_s = \exp\left[-8\pi^2\gamma^2\right] \tag{12}$$

where γ is the roughness factor, given as

$$\gamma = \frac{\varsigma_h \sin\psi_g}{\lambda} \tag{13}$$

where ς_h is the standard deviation of the reflecting surface heights.

III. THE PROPOSED METHOD

In this section, a novel sparse representation framework based target localization algorithm, combined with dictionary refinement technique [32] and alternatingly iterative scheme [33], is proposed for complex terrain environment with a limited number of snapshots. The algorithm mainly consists of three steps. After signal component is extracted via low-rank decomposition technique, the signal component is used to obtain the target elevation angle based on sparse representation framework. Finally, target altitude is calculated with the estimated elevation angle. The details of this proposed algorithm are described in the following subsections.

A. OVERCOMPLETE REPRESENTATION WITH MULTIPLE SNAPSHOTS

Noting the sparsity of the signals in the elevation direction, we start to formulate the problem mentioned in Section II as a sparse representation problem. Specially, it is worth mentioning that the multipath attenuation coefficient should be taken into account in order to exploit the multipath structure information sufficiently and also to enhance the inner structure of the overcomplete dictionary. By considering these factors, an overcomplete dictionary $\mathbf{B}_{\mathbf{\Omega}}$ of size $M \times V$ is constructed, which can be expressed as

$$\mathbf{B}_{\mathbf{\Omega}} = \left[\mathbf{b}\left(\boldsymbol{\zeta}_1\right), \mathbf{b}\left(\boldsymbol{\zeta}_2\right), \cdots, \mathbf{b}\left(\boldsymbol{\zeta}_v\right), \cdots, \mathbf{b}\left(\boldsymbol{\zeta}_V\right)\right] \tag{14}$$

where $\mathbf{\Omega}$ is the parameter set,

$$\mathbf{\Omega} = \left\{ \boldsymbol{\zeta}_v \triangleq \left(\theta_{d,v}, \theta_{s,v}, \rho_v, \Delta R_v\right) \middle| \theta_{d,v} \in \boldsymbol{\theta}_{d,\text{set}}, \theta_{s,v} \in \boldsymbol{\theta}_{s,\text{set}}, \rho_v \in \boldsymbol{\rho}_{\text{set}}, \Delta R_v \in \Delta\mathbf{R}_{\text{set}}, v = 1, 2, \cdots, V \right\} \tag{15}$$

where $\boldsymbol{\theta}_{d,\text{set}}$, $\boldsymbol{\theta}_{s,\text{set}}$, $\boldsymbol{\rho}_{\text{set}}$ and $\Delta\mathbf{R}_{\text{set}}$ are the given parameter sets of $\theta_{d,v}$, $\theta_{s,v}$, ρ_v and ΔR_v, respectively. $V = |\mathbf{\Omega}|$ is the cardinality of $\mathbf{\Omega}$ with the assumption of $V \gg M$. $\mathbf{b}\left(\boldsymbol{\zeta}_v\right)$ is the v-th atom of $\mathbf{B}_{\mathbf{\Omega}}$:

$$\mathbf{b}\left(\boldsymbol{\zeta}_v\right) = \mathbf{a}\left(\theta_{d,v}\right) + \rho_v e^{-j2\pi\,\Delta R_v/\lambda}\mathbf{a}\left(\theta_{s,v}\right), \tag{16}$$

where $\mathbf{a}\left(\theta_{d,v}\right)$ and $\mathbf{a}\left(\theta_{s,v}\right)$ denote the steering vectors of the array toward directions of $\theta_{d,v}$ and $\theta_{s,v}$, respectively, and

$$\mathbf{a}\left(\theta\right) = \left[1, e^{-j2\pi d\,\sin(\theta)/\lambda}, \cdots, e^{-j(M-1)2\pi d\,\sin(\theta)/\lambda}\right]^T \tag{17}$$

where d is the inter-element distance of two adjacent elements. Then, by using an overcomplete representation, the problem in (7) can be reformulated into the form:

$$\begin{aligned}\mathbf{x}\left(t\right) &= a\left[\mathbf{a}\left(\theta_d\right) + \bar{\rho}\mathbf{a}\left(\theta_s\right)\right]s\left(t\right) + \mathbf{n}\left(t\right) \\ &= \mathbf{B}_{\mathbf{\Omega}}\boldsymbol{\omega}\left(t\right) + \mathbf{n}\left(t\right), \quad t \in \{t_1, \cdots, t_L\}\end{aligned} \tag{18}$$

where $\boldsymbol{\omega}(t) = \left[\omega_1\left(t\right), \cdots, \omega_v\left(t\right), \cdots, \omega_V\left(t\right)\right]^T$ is the spatial sparse coefficient vector and the v-th element $\omega_v\left(t\right)$ is $as(t)$ if the v-th atom of $\mathbf{B}_{\mathbf{\Omega}}$ contains the parameter set $\left\{\theta_{d,v}, \theta_{s,v}, \rho_v, \Delta R_v\right\}$ corresponding to a real target, and zero otherwise, and $\bar{\rho}$ is defined in (6).

Because target localization with multi-snapshots in multipath propagation environment is of great practical importance, we consider multi-snapshots at time instants $t_1, \cdots, t_L$. Since the transmitted waveform is narrowband, e.g., the bandwidth of the experimental radar system used to collect real data in Section IV is 1MHz, it is assumed that the motion of a target is not taken into consideration during the observation time of one CPI, or in other words, the motion of a target can be neglected during the time interval $\{t_1, \cdots, t_L\}$. Let

$$\mathbf{X} = [\mathbf{x}(t_1), \cdots, \mathbf{x}(t_l), \cdots, \mathbf{x}(t_L)] \tag{19}$$

be the measurement data matrix, and define

$$\mathbf{W} = \left[\boldsymbol{\omega}\left(t_1\right), \cdots, \boldsymbol{\omega}\left(t_l\right), \cdots, \boldsymbol{\omega}\left(t_L\right)\right] \tag{20}$$

and

$$\mathbf{N} = \left[\mathbf{n}\left(t_1\right), \cdots, \mathbf{n}\left(t_l\right), \cdots, \mathbf{n}\left(t_L\right)\right]. \tag{21}$$

Then, by using (18), (20) and (21), (19) can be easily rewritten as

$$\begin{aligned}\mathbf{X} &= [\mathbf{x}(t_1), \cdots, \mathbf{x}(t_l), \cdots, \mathbf{x}(t_L)] \\ &= \left[\begin{array}{c}\left(\mathbf{B}_{\mathbf{\Omega}}\boldsymbol{\omega}\left(t_1\right) + \mathbf{n}\left(t_1\right)\right), \cdots, \left(\mathbf{B}_{\mathbf{\Omega}}\boldsymbol{\omega}\left(t_l\right) + \mathbf{n}\left(t_l\right)\right), \\ \cdots, \left(\mathbf{B}_{\mathbf{\Omega}}\boldsymbol{\omega}\left(t_L\right) + \mathbf{n}\left(t_L\right)\right)\end{array}\right] \\ &= \mathbf{B}_{\mathbf{\Omega}}\mathbf{W} + \mathbf{N}.\end{aligned} \tag{22}$$

In fact, this overcomplete representation allows us to convert the problem of direction estimation into the problem of sparse spectrum estimation. The solution of the following optimization may provide an estimate:

$$\min_{\mathbf{W}} \ \|\mathbf{X} - \mathbf{B}_{\mathbf{\Omega}}\mathbf{W}\|_2^2 + e\,\|\mathbf{W}\|_0 \tag{23}$$

where e controls the tradeoff between the data fitting term and the sparsity term. A variety of iterative greedy algorithms including Orthogonal Matching Pursuit (OMP) [34], [35], Newtonized OMP (NOMP) [36] and multi-snapshot Newtonized (MNOMP) [37] have been proposed to obtain an approximate solution to problem (23). In the previous work [36], it has been shown that the frequencies and amplitudes of a noisy mixture of sinusoids can be efficiently estimated by using the MNOMP algorithm. However, the computational complexity of the standard OMP technique increases linearly with L. Thus, with the increasing number of snapshots, this approach may not work in real-time applications.

B. EXTRACTION OF SIGNAL COMPONENT VIA LOW-RNAK DECOMPOSITION

Let us consider a common practical case in which there is only one target. Because the spatial signals are coherent with each other, the rank of $\mathbf{X}$ in (19) should be ideal if the noise component $\{\mathbf{n}(t_l)\}_{l=1}^{L}$ in $\mathbf{X}$ is neglected (*Proof:* See Appendix A). This means that the received data $\{\mathbf{x}(t_l)\}_{l=1}^{L}$ should lie in a one-dimensional signal subspace. Motivated by this, a low-rank decomposition operation is implemented for $\mathbf{X}$ in order to reduce both the signal dimension and the sensitivity to noise. Consider the singular value decomposition (SVD) of $\mathbf{X}$

$$\mathbf{X} = \mathbf{U}_{\mathrm{X}}\mathbf{\Sigma}_{\mathrm{X}}\mathbf{V}_{\mathrm{X}}^{H}. \tag{24}$$

Since the data points (i.e., columns vectors of $\mathbf{X}$) lie in a single one-dimensional signal subspace, or in other words, the range space of the noiseless data in $\mathbf{X}$ is spanned by only one singular vector, it is reasonable to represent the range space of $\mathbf{X}$ by using the singular vector corresponding to the largest singular value. Thus, a reduced-dimensional basis for the signal subspace, $\mathbf{y}_{\mathrm{SV}}$, which has the most signal power, can be formulated as

$$\mathbf{y}_{\mathrm{SV}} = \mathbf{U}_{\mathrm{X}}\mathbf{\Sigma}_{\mathrm{X}}\mathbf{h}_c \tag{25}$$

where $\mathbf{h}_c$ is a vector of size $L \times 1$ with its first entry being one, and the others zeros. If we calculate the correlation matrix of the data $\mathbf{X}$, i.e.,

$$\begin{aligned}\mathbf{R}_{\mathrm{X}} &= E\left(\mathbf{X}\mathbf{X}^{H}\right)\\ &= a^2\sigma_s^2\left[\mathbf{a}(\theta_d) + \bar{\rho}\mathbf{a}(\theta_s)\right]\left[\mathbf{a}(\theta_d) + \bar{\rho}\mathbf{a}(\theta_s)\right]^{H} + \mathbf{R}_{\mathrm{n}}\end{aligned} \tag{26}$$

where $\sigma_s^2 = \frac{1}{L}\sum_{l=1}^{L} s(t_l)\, s^*(t_l)$ denotes the signal power, and $\mathbf{R}_{\mathrm{n}}$ is the noise covariance matrix. It is seen from (26) that the noiseless signals lie in a one-dimensional subspace, which also justifies our discussion of the reduced-dimensional basis $\mathbf{y}_{\mathrm{SV}}$.

We would like to emphasize that a low-rank decomposition operation on the $M \times L$ radar observation data matrix $\mathbf{X}$ is essentially different from the motivation of the rank-one constraint utilized in [25]. The above SVD operation is directly implemented to the observation data in order to keep the signal subspace only and reduce the data dimension. However, the motivation of using the rank-1 constraint for the signal matrix $\mathbf{A} = \tilde{\mathbf{a}}\tilde{\mathbf{a}}^{T}$ (not the radar observation data) in [25] is to estimate the directional vector $\tilde{\mathbf{a}}$ that contains the information of target direction from the radar observation data. Particularly, we mentioned in Section I that both the multipath attenuation coefficient and the coherency structure information of the spatial signals are not taken into consideration in [25]. In contrast, the inner structure information of the spatial signals is sufficiently exploited in this paper by introducing a parametric adaptive dictionary $\mathbf{B}_{\mathbf{\Omega}}$ that is defined in (14), and the target localization performance can be improved by exploiting the multipath structure information. Because the rank-1 constraint can be also imposed in (26), which is similar to that we used in [25], some comparisons of localizing a target from the correlation matrix $\mathbf{X}\mathbf{X}^{H}$ by using the method in [25] will be presented in Section IV in order to compare the performances of the two low-angle target localization algorithms.

C. TARGET LOCALIZATION BASED ON SPARSE REPRESENTATION WITH STRUCTURAL DICTIONARY

Our goal is to estimate the unknown location θ_d corresponding to the real target from $\mathbf{y}_{\mathrm{SV}}$ described in Section III-B. By introducing the structural adaptive dictionary $\mathbf{B}_{\mathbf{\Omega}}$, the inner structural information can be sufficiently utilized and the sparsity of the spatial signals is reduced to be one. In fact, $\mathbf{y}_{\mathrm{SV}} = \mathbf{U}_{\mathrm{X}}\mathbf{\Sigma}_{\mathrm{X}}\mathbf{h}_c = \mathbf{X}\mathbf{V}_{\mathrm{X}}\mathbf{h}_c$. Let $\boldsymbol{\varepsilon} = \mathbf{W}\mathbf{V}_{\mathrm{X}}\mathbf{h}_c$ and $\mathbf{n}_{\mathrm{SV}} = \mathbf{N}\mathbf{V}_{\mathrm{X}}\mathbf{h}_c$, (22) can be simplified into

$$\mathbf{y}_{\mathrm{SV}} = \mathbf{B}_{\mathbf{\Omega}}\boldsymbol{\varepsilon} + \mathbf{n}_{\mathrm{SV}}. \tag{27}$$

Correspondingly, due to the fact that there is only one target and the sparsity of the spatial signals is reduced to one, the matrix $\mathbf{W}$ has only one non-zero row and all the other rows are zeros. Thus, with only one nonzero entry in $\boldsymbol{\varepsilon}$, the problem in (23) can be reformulated to the following L_0-minimization problem

$$\begin{aligned}\hat{\boldsymbol{\varepsilon}} = \arg\min_{\boldsymbol{\varepsilon}} \ & \|\mathbf{y}_{\mathrm{SV}} - \mathbf{B}_{\mathbf{\Omega}}\boldsymbol{\varepsilon}\|_2^2\\ \text{s.t.} \ & \|\boldsymbol{\varepsilon}\|_0 = 1\end{aligned} \tag{28}$$

where $\hat{\boldsymbol{\varepsilon}}$ is the estimated sparse coefficient vector with respect to dictionary $\mathbf{B}_{\mathbf{\Omega}}$. By solving (28), the estimation of the target direction can be achieved at the same time. Unfortunately, the target location estimated by the cost function in (28) may not exist in practice. This is mainly because the searching grid for an overcomplete dictionary $\mathbf{B}_{\mathbf{\Omega}}$ cannot be too dense due to the four dimensional searching. Furthermore, because of the maneuverability of a target and the time variance of the multipath interference, it is difficult to use a fixed dictionary to satisfy various terrain conditions [38]. To address the problem mentioned above, a framework for adaptive joint target localization and dictionary refinement is introduced in the following subsection.

D. PRARMETER ESTIMATE WITH ALTERNATING ITERATION AND DICTIONARY REFINEMENT

Considering the high dimension of the parameterized dictionary $\mathbf{B}_{\mathbf{\Omega}}$, it is impractical to use fine dictionary grid size uniformly due to the high computational complexity. In order to keep a balance between the estimation accuracy of signal reconstruction and the computational complexity, a novel technique based on alternating iteration and dictionary refinement is explored for adaptively refining the grid size. An overview of the proposed algorithm is depicted in Fig. 2.

The proposed target localization procedure can be divided into three stages. In the first and second stages, a fixed dictionary of smaller dimension is utilized to achieve preliminary

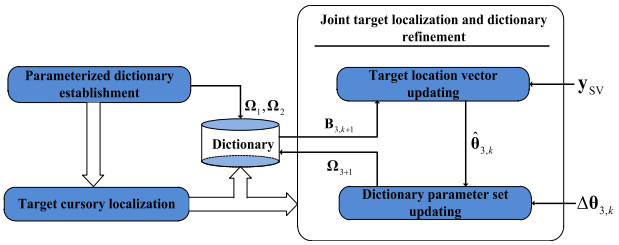

FIGURE 2. An overview of the proposed algorithm, where $\mathbf{y_{SV}}$ denotes the extraction of signal component from the array measurement data $\mathbf{X}$, Ω_1 and Ω_2 denote the initially coarse parameter sets of dictionaries, $\hat{\theta}_{3,k}$, $\Delta\theta_{3,k}$, $\Omega_{3,k+1}$ and $\mathbf{B}_{\Omega_{3,k+1}}$ denote the current updating parameter vector, the parametric grid set, the refined parameter set and the refined dictionary in the $(k+1)$-th iteration, respectively.

target localization. In the third stage, we update the dictionary with the refined grid only around the detected target location. A brief description of parameter estimation in each stage is shown in Table 1.

TABLE 1. A brief description of parameter estimation in each stage.

Stage No.	Estimated parameters
1	Coarse estimation of (θ_d, θ_s)
2	Coarse estimation of $(\rho, \Delta R)$
3	Improved estimation of $(\theta_d, \theta_s, \rho, \Delta R)$

Without loss of generality, the direction parameters θ_d and θ_s are extracted firstly when the ideal symmetric multipath model can be utilized for the initialization of directions of target and its image. Subsequently, ρ and ΔR are introduced as unknown parameters for preliminary target localization in Stage 2. Finally, the adaptive dictionary refinement and the accurate target localization can be realized by using alternatingly iterative and dictionary refinement. The details of these stages are explained as follows.

Stage 1 (Coarse Estimation of (θ_d, θ_s)): By implementing the ideal symmetric multipath model, the coarse parameter set $\mathbf{\Omega}_1$ can be obtained by

$$\mathbf{\Omega}_1 = \left\{ \boldsymbol{\zeta}_{v_1} \triangleq \left(\theta_{d,v_1}, \theta_{s,v_1}, \rho_{v_1}, \Delta R_{v_1}\right) \middle| \theta_{d,v_1} \in \boldsymbol{\theta}_{d,\text{set}}, \atop \theta_{s,v_1} = -\theta_{d,v_1}, \rho_{v_1} = \rho_0, \Delta R_{v_1} = \Delta R_0, v_1 = 1, 2, \cdots, V_1 \right\} \tag{29}$$

where $V_1 = |\mathbf{\Omega}_1|$ is the cardinality of $\mathbf{\Omega}_1$, ρ_0 and ΔR_0 are the reflection coefficient and the path difference for the ideal smooth reflecting surface, respectively. Generally, ρ_0 is regarded as $0.9\exp(j\pi)$, and ΔR_0 can be easily computed by setting $h_g = 0$ and $\alpha = 0$. Then, the corresponding dictionary $\mathbf{B}_{\mathbf{\Omega}_1}$ that is similarly constructed as $\mathbf{B}_{\mathbf{\Omega}}$ in (14) and the sparse coefficient vector $\hat{\boldsymbol{\varepsilon}}_1$ can be estimated by solving (28), where $\mathbf{\Omega}$ is replaced with $\mathbf{\Omega}_1$. The index $\hat{v}_1$ of the non-entry in $\hat{\boldsymbol{\varepsilon}}_1$ represents the information of the parameters corresponding to a real target, which can be calculated as

$$\hat{v}_1 = \arg\max_{v_1} \left|\hat{\boldsymbol{\varepsilon}}_1(v_1)\right| \tag{30}$$

where $\hat{\boldsymbol{\varepsilon}}_1(v_1)$ is the v_1-th element of vector $\hat{\boldsymbol{\varepsilon}}_1$ and $v_1 = 1, 2, \cdots, V_1$. Then, the coarse estimation of the direction parameters (θ_d, θ_s), denoted as $\hat{\boldsymbol{\theta}}_1$, can be correspondingly obtained from $\boldsymbol{\zeta}_{\hat{v}_1}$, which denotes the $\hat{v}_1$-th element of $\mathbf{\Omega}_1$.

Stage 2 (Coarse Estimation of $(\rho, \Delta R)$ Based on $\hat{\boldsymbol{\theta}}_1$): In this stage, the parameters $(\rho, \Delta R)$ are treated as unknown and can be roughly estimated by incorporating them in the following coarse parameter set $\mathbf{\Omega}_2$,

$$\mathbf{\Omega}_2 = \left\{ \boldsymbol{\zeta}_{v_2} \triangleq \left(\theta_{d,v_2}, \theta_{s,v_2}, \rho_{v_2}, \Delta R_{v_2}\right) \middle| \left(\theta_{d,v_2}, \theta_{s,v_2}\right) \in \hat{\boldsymbol{\theta}}_1, \atop \rho_{v_2} \in \tilde{\boldsymbol{\rho}}_{\text{set}}, \Delta R_{v_2} \in \Delta\tilde{\mathbf{R}}_{\text{set}}, v_2 = 1, 2, \cdots, V_2 \right\} \tag{31}$$

where $V_2 = |\mathbf{\Omega}_2|$ is the cardinality of $\mathbf{\Omega}_2$, $\tilde{\boldsymbol{\rho}}_{\text{set}}$ and $\Delta\tilde{\mathbf{R}}_{\text{set}}$ are the given parameter sets of ρ_{v_2} and ΔR_{v_2} for searching, respectively. Similar to the process presented in Stage 1, the updated sparse coefficient vector $\hat{\boldsymbol{\varepsilon}}_2$ and the index $\hat{v}_2$ of nonzero entry in $\hat{\boldsymbol{\varepsilon}}_2$ can be achieved by solving (28) and (30), where $\mathbf{\Omega}$ is replaced with $\mathbf{\Omega}_2$ and $\hat{\boldsymbol{\varepsilon}}_1(v_1)$ is replaced with $\hat{\boldsymbol{\varepsilon}}_2(v_2)$, respectively. Then, the preliminary estimation of target location parameters $(\theta_d, \theta_s, \rho, \Delta R)$, denoted as $\hat{\boldsymbol{\theta}}_2$, can be obtained as $\hat{\boldsymbol{\theta}}_2 = \boldsymbol{\zeta}_{\hat{v}_2}$, where $\boldsymbol{\zeta}_{\hat{v}_2}$ denotes the $\hat{v}_2$-th element of $\mathbf{\Omega}_2$.

Stage 3 (Joint Adaptive Dictionary Refinement and Accurate Target Localization): Instead of creating a fine searching grid over the entire parameter interval, we refine the grid only around the detected location where the target may appear. The accuracy of the target location is then improved by alternating dictionary refinement and target location parameter update. The details are described below.

Let us denote $\mathbf{\Omega}_{3,k+1}$ and $\Delta\boldsymbol{\theta}_{3,k}$ as the parameter set and the parametric grid set in the $(k+1)$-th iteration, respectively, where $k = 0, \cdots, K-1$, and K is the maximum number of iterations. In the dictionary refinement process, the updated parameter set $\mathbf{\Omega}_{3,k+1}$ can be firstly obtained by picking an interval $\Delta\boldsymbol{\theta}_{3,k}$ around $\hat{\boldsymbol{\theta}}_{3,k}$, i.e., let $\hat{\boldsymbol{\theta}}_{3,0} = \hat{\boldsymbol{\theta}}_2$ when $k = 0$. Then, similar to the process presented in Stage 1 and Stage 2, the $(k+1)$-th updated target location parameters can be determined from the support index of $\hat{\boldsymbol{\varepsilon}}_{3,k+1}$ and the estimation set $\hat{\boldsymbol{\theta}}_{3,k}$ can be simultaneously refined as $\hat{\boldsymbol{\theta}}_{3,k+1} = \left[\hat{\theta}_{d,k+1}, \hat{\theta}_{s,k+1}, \hat{\rho}_{k+1}, \Delta\hat{R}_{k+1}\right]$. After updating the grid $\Delta\boldsymbol{\theta}_{3,k}$ and the parameter set $\mathbf{\Omega}_{3,k+1}$, we repeat the aforementioned procedure until the iteration stopping condition is satisfied. A commonly used halting criterion is adopted for this approach, i.e., the variation of the residual energy between two consecutive iterations is smaller than a pre-given threshold χ or the number of iterations has reached the upper limit K.

Let us now clarify some details of the algorithm. When update the parameter set $\mathbf{\Omega}_{3,k+1}$ at step $k+1$ in Stage 3, we pick an interval around the location where the target is present based on $\hat{\boldsymbol{\theta}}_{3,k}$, which includes a spacing of two grids on either

side. In addition, for the grid refinement of $\Delta\boldsymbol{\theta}_{3,k}$ in Stage 3, the new grid size is selected as a fraction of the previous one in the interval, i.e., $\Delta\boldsymbol{\theta}_{3,k+1} = \Delta\boldsymbol{\theta}_{3,k}/\varpi$. Since it has been verified that the approach of slowly shrinking $\Delta\boldsymbol{\theta}_{3,k}$, which corresponding to small ϖ and more refinement steps, is more numerically stable according to both simulation and measured data, therefore, ϖ is chosen as a relatively small number, e.g., 1.5, in our experiments.

E. ALTITUDE ESTIMATION ACCURACY

After the iteration terminates, the target altitude can be obtained with the final estimation of the real target direction $\hat{\theta}_d$ obtained in Section III-D. Considering the influence of the curvature of the Earth, the calculation of the target altitude can be divided into the following two cases. For a short-range target, i.e., a few dozens of kilometers, the target altitude can be obtained by

$$\hat{h}_t = R_d \sin\hat{\theta}_d + h_a, \tag{32}$$

while for a long-range target, i.e., a few hundreds of kilometers, the calculation of the target altitude can be expressed as

$$\hat{h}_t = R_d \sin\hat{\theta}_d + R_d \big/ 2R_e + h_a \tag{33}$$

where R_e is the effective radius of the earth, which is usually set as $R_e = 4R_0/3$ and $R_0 = 6370$km denotes the real radius of the Earth.

In summary, the proposed low-angle target localization algorithm is listed in Table 2.

TABLE 2. The proposed algorithm for target localization.

Initialization: Set the maximum number of iterations K, $k=0$, $\mu_0=0$, $\mu_1=1$, $\chi=10^{-6}$, $\Delta\boldsymbol{\theta}_{3,k}=\Delta\boldsymbol{\theta}_0$, where χ is the threshold of relative change of the residue energy between consecutive iterations, $\Delta\boldsymbol{\theta}_0$ is the initial parametric grid size. Let μ_k denote the residue energy at the k-th iteration.

Coarse estimation of parameter set :

1-1) Implement the ideal symmetric multipath model, estimate the parameters (θ_d, θ_s) coarsely by (28)—(30), and obtain the parameter set $\hat{\boldsymbol{\theta}}_1$;

1-2) Construct dictionary $\mathbf{B}_{\boldsymbol{\Omega}_2}$ by (31) and (14), estimate $(\rho, \Delta R)$ according to (28) and (30) based on $\hat{\boldsymbol{\theta}}_1$, and obtain the parameter set $\hat{\boldsymbol{\theta}}_2$;

Joint target localization and dictionary refinement:

While $|\mu_{k+1} - \mu_k| > \chi$

2-1) Update the parameter set $\boldsymbol{\Omega}_{3,k+1}$ based on $\hat{\boldsymbol{\theta}}_{3,k}$ and $\Delta\boldsymbol{\theta}_{3,k}$, construct the updated dictionary $\mathbf{B}_{\boldsymbol{\Omega}_{3,k+1}}$ similar to the process presented in Stage 1 and Stage 2;

2-2) Calculate $\hat{\boldsymbol{\varepsilon}}_{3,k+1}$ according to (28) by using $\mathbf{B}_{\boldsymbol{\Omega}_{3,k+1}}$, then estimate the parameters corresponding to a real target: $\hat{\boldsymbol{\theta}}_{3,k+1} = \boldsymbol{\zeta}_{\hat{v}_{3,k+1}}$, where $\hat{v}_{3,k+1} = \arg\max_{v_{3,k+1}} \left|\hat{\boldsymbol{\varepsilon}}_{3,k+1}(v_{3,k+1})\right|$, $\boldsymbol{\zeta}_{\hat{v}_{3,k+1}}$ is the $\hat{v}_{3,k+1}$-th element of the parameter set $\boldsymbol{\Omega}_{3,k+1}$;

2-3) If the maximum number of the iterations is reached, stop the iteration; Else, refine the parameter grid size $\Delta\boldsymbol{\theta}_{3,k+1} = \Delta\boldsymbol{\theta}_{3,k}/\varpi$ with $\varpi = 1.5$, and set $k = k+1$. Go to step 2-1).

End

Calculate the target altitude by (32) or (33) with the knowledge of the target range and the antenna height.

The computational complexity of the proposed method is briefly analyzed as follows. For the matrix SVD step, its complexity is $O\left(R_1R_2^2 + R_1^2R_2 + R_1^3\right)$ for a matrix of size $R_1 \times R_2$ [39]. Hence, the computational cost of extraction of the signal component is $O\left(M^3 + M^2L + ML^2\right)$. Assume that the dimensions of the dictionaries used in Stage 1 and Stage 2 in Section III-D are $M \times N_1$ and $M \times N_2$, respectively. Then, the corresponding computational costs are $O\left(N_1M^2\right)$ and $O\left(N_2M^2\right)$, respectively. In Stage 3, because two grid spacing are introduced to either side of the peak of the sparse spectrum, the dimensions of the adaptive dictionaries in each iteration is 5^4. The corresponding computational cost is $O\left(5^4QM^2\right)$, where Q is the number of iterations when the algorithm is stopped. Therefore, the overall computational complexity of the proposed algorithm is $O\left(M^3 + \left(N_1 + N_2 + 5^4Q + L\right)M^2 + ML^2\right)$. In our simulations, after a few (e.g. 8) iterations of adaptive refinement, the grid becomes fine enough to satisfy the estimated accuracy and the effect of the grid size can be negligible.

IV. SIMULATION RESULTS AND MEASURED DATA VALIDATION

A. SIMULATION RESULTS

For performance studies on various scenarios, e.g., those with different reflecting surfaces and/or different numbers of snapshots, several simulations are performed to illustrate the performance of the proposed low-angle target localization algorithm in this subsection. In all the presented simulations, a uniform linear array (ULA) is considered, which comprises $M = 16$ isotropic elements separated with one half-wavelength, i.e., $\lambda/2 = 0.5$ m. It is worth mentioning that the ideal array is assumed and the array error is not considered in this paper. A few comparisons are made with other existing state-of-the-art algorithms, i.e., the forward/backward spatial smoothing MUSIC (SSMUSIC) algorithm [6], the subspace based method in [12], the relax algorithm [15], the AP-ML algorithm [19], the RML algorithm [20] and the rank-1 based method in [25] to assess the performance merits of the proposed algorithm. The Cramér-Rao bound for the target's DOA, derived in Appendix B, is utilized as an optimization criterion for the target localization scheme. In addition, the SNR in our simulations is defined as

$$\mathrm{SNR} = 10\lg\left(P_s \big/ \sigma_N^2\right) \tag{34}$$

where P_s is the received average signal power, and σ_N^2 is the noise power. All the experiments are performed using MATLAB R2011b on a PC with Intel i7-4770, core frequency 3.40GHz and RAM 8G. The estimation performance of the target parameters is evaluated in terms of root mean square error (RMSE), which is defined as

$$\mathrm{RMSE}_{\theta_d} = \sqrt{\frac{1}{U}\sum_{u=1}^{U}\left(\hat{\theta}_{d,u} - \theta_d\right)^2} \tag{35}$$

and

$$\mathrm{RMSE}_{h_t} = \sqrt{\frac{1}{U}\sum_{u=1}^{U}\left(\hat{h}_{t,u} - h_t\right)^2} \tag{36}$$

where U is the total number of Monte Carlo trials, $\hat{\theta}_{d,u}$ and $\hat{h}_{t,u}$ are the estimated target direction and target altitude in the u-th trial, respectively.

The first simulation is to examine the performance of the proposed algorithm in a scenario with an ideal smooth reflecting surface and a sufficient number of snapshots. Similar to most existing methods, the height of the reflecting surface, the included angle and the specular reflection coefficient are set to 0, 0° and $0.9\exp(j\pi)$, respectively. The height of the radar location is set as 100m, the target is located at 125km away with an altitude of 3km for Fig. 3(a) and (b) and 6km for Fig. 3(c) and (d), respectively. These parameter settings produce the direct angle $\theta_d = 1.33^\circ$, the indirect angle $\theta_s = -1.41^\circ$, the grazing angle $\psi_g = 1.41^\circ$ for Fig. 3(a) and (b), and the direct angle $\theta_d = 2.71^\circ$, the indirect angle $\theta_s = -2.79^\circ$, the grazing angle $\psi_g = 2.79^\circ$ for Fig. 3(c) and (d), respectively. In this simulation, the number of available snapshots is 128, and the SSMUSIC algorithm is applied by using twelve-sensor subarrays. Fig. 3 shows the RMSEs of target direction and target altitude. Each statistical result is averaged over 500 independent Monte Carlo trials for each SNR value.

It can be observed from Fig. 3(a) – (d) that the SSMUSIC algorithm performs poorly in various target altitude conditions because the spatial smoothing operation produces the loss of effective array aperture to degrade the angular resolution. Except for the method in [12] and the proposed algorithm in Fig. 3(a) and (b), the performances of all the other methods are severely impacted when the elevation angle is less than 1/4 beamwidth even in high SNR condition. This phenomenon indicates that the method in [12] and the proposed algorithm have the abilities to distinguish the real target in lower elevation angle. This is probably because that the inherent structure information of the target and its image is sufficiently exploited in the two algorithms. In Fig. 3(c) and (d), we can see that the performances of all the algorithms, except the SSMUSIC algorithm, are almost the same, which indicates that these algorithms can provide effective performance for target localization when the target has a relatively high altitude under the ideal scenario, i.e., that used in this simulation. It can also be seen from Fig. 3(a) and (c) that the RMSEs of both the method in [12] and the proposed algorithm can closely approach the corresponding CRB for the ideal symmetric multipath scenario when SNR is greater than 10dB. In particular, when comparing Fig. 3(b) and (d), it is clear that the higher altitude of the target, the smaller estimated RMSE of the target altitude can be achieved for each SNR. This is because the angle-interval between the real target and its multipath image is getting bigger with the increase of the target altitude.

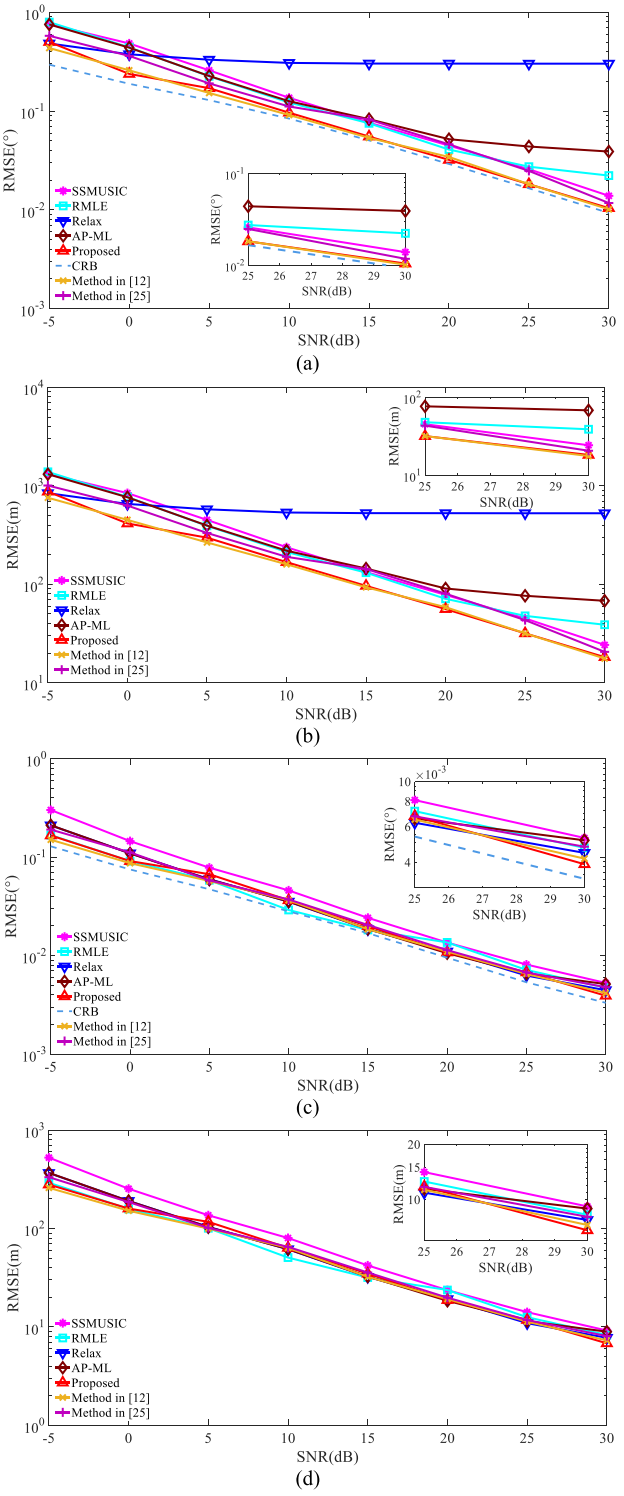

FIGURE 3. RMSE results of respective algorithms versus SNR using 128 snapshots with an ideal smooth reflecting surface. (a) target DOA estimation for h_t=3km; (b) target altitude estimation for h_t=3km; (c) target DOA estimation for h_t=6km; (d) target altitude estimation for h_t=6km. All results are averaged over 500 Monte Carlo trials.

A comparison for the average running times of the respective algorithms is also demonstrated in Table 3. The searching region of the elevation angle is set as [0°, 10°]. It is clear

TABLE 3. Average running times of different algorithms (Sec).

Algorithm	Search Interval (deg.)	Runtime (sec.)	Algorithm	Search Interval (deg.)	Runtime (sec.)
SSMUSIC	0.01	0.35	Method in [12]	0.01	2.69
	0.001	1.56		0.001	10.65
RML	0.01	0.51	Method in [25]	0.01	2.13
	0.001	4.69		0.001	12.69
Relax	0.01	5.02	Our Method	0.01	**1.33**
	0.001	27.36		0.001	**6.11**
AP-ML	0.01	1.62	-	-	-
	0.001	25.25			

that the relax algorithm is time-consuming since a recursive searching is required. The SSMUSIC method and the RML method are the two most computationally efficient algorithms. This is because only one dimensional searching is required after the fixed geometry relationship is introduced. In other words, these two algorithms are competitive in the scenario with ideal smooth reflecting surface. The running time of the proposed algorithm is more than that of the SSMUSIC algorithm and the RML algorithm. This is because in Stage 3 of our proposed algorithm, the dictionary parameters are refined by a gradual approach, which produces a more accurate and stable estimation of target altitude at the cost of additional computation time. In particular, it is worth mentioning that the running times of the AP-ML algorithm and the relax algorithm increase rapidly with the increased density of the search grid while the running times of the SSMUSIC algorithm, the RML algorithm, the method in [12], the method in [25] and the proposed algorithm do not.

Because the computational complexity of the method in [25] cannot be expressed in theory, the analysis of computational complexities of the other six algorithms is summarized in Table 4. In Table 4, M_{array} is the number of subarrays, M_{sub} denotes the number of sensors in each subarray, K is the iteration number, J and J_ρ represent the number of angle grids and the number of reflection coefficient grids, respectively.

TABLE 4. Computational complexity comparisons.

Algorithm	Computational Complexity	Algorithm	Computational Complexity
SSMUSIC	$O\left\{\begin{matrix}\left(L+2M_{array}M_{sub}\right)M^2+\\ \left(M+3+2J\right)M_{sub}^2-3M_{sub}\end{matrix}\right\}$	AP-ML	$O\left\{4K\left[2M^3+M^2+4M\right]+LM^2\right\}$
RML	$O\left\{J\left[\left(L+8\right)M^2+\left(L^2+8\right)M+3L^3\right]\right\}$	Method in [12]	$O\left\{\begin{matrix}3M^3+\left(\begin{matrix}L+4J+\\ 4KJ+8KJ_\rho\end{matrix}\right)\times\\ M^2+\left(4J+16KJ_\rho\right)M\end{matrix}\right\}$
Relax	$O\left\{2K\left[4JM^3+\left(2L+J\right)M^2+ML\right]\right\}$	Our Method	$O\left\{\begin{matrix}M^3+\left(N_1+N_2+5^4Q+L\right)\times\\ M^2+ML^2\end{matrix}\right\}$

To better illustrate the performances of the respective algorithms mentioned in the previous simulation, a complex scenario with horizontal reflecting surface is introduced in the second simulation, while the height of the reflecting surface is unknown. In particular, considering a case of limited observation time, the number of available snapshots is reduced to 32 in this simulation. The SSMUSIC algorithm is also applied by using twelve-sensor subarrays. Assume that the multipath wave illuminates a dry ground surface where its relative dielectric constant ε_r, standard deviation ς_h and conductivity δ are 7, 0.3m and 1×10^{-5} S/m, respectively. The height of reflecting surface and the included angle are 10m and 0°, respectively. In addition, the radar height is 100m and the vertical polarization pattern is utilized. The target is located at 125km away with an altitude of 4km for Fig. 4(a) and (b) and 5km for Fig. 4(c) and (d) respectively. Fig. 4 depicts the RMSEs of target direction and target altitude versus different SNR values, where the results are averaged over 500 independent trials.

It is observed from Fig. 4 that the RML algorithm does not perform as well as the other six algorithms when SNR is larger than 5dB. In other words, the RML algorithm can hardly identify the location of the real target even in high SNR condition. This is because the commonly utilized deterministic multipath signal model produces mismatch for the complex scenario used in this simulation. It can also be noticed that the SSMUSIC algorithm and the method in [12] achieve the performances slightly inferior to the relax algorithm, the AP-ML algorithm, the method in [25] and the proposed algorithm, possibly because the limited number of snapshots just provides a relative low SNR and results in an inaccurate estimate of the sample covariance matrix. Fig. 4 also reveals that the method in [25], the AP-ML algorithm, and the relax algorithm show almost the same performance and the proposed algorithm slightly outperforms all the other algorithms in high SNR conditions. In particular, it is worth mentioning that the proposed algorithm almost approaches the corresponding CRB for the complex multipath scenario when SNR is larger than 10dB in Fig. 4(a) and (c). These results indicate that the proposed algorithm can provide effective performance for low-angle target localization in the complex scenario without any prior information about the reflected multipath.

In order to examine the behavior of respective algorithms in a more complex or generalized scenario, our last simulation is to extend the consideration of the following condition. A terrain with sloped reflecting surface is introduced, as shown in Fig. 1, where both the height of the reflecting surface h_g and the included angle α are unknown beforehand. Especially, a more complex scenario with only ten available snapshots is taken into consideration to examine the abilities of the algorithms in the environment of small sample size. Assume that the height of reflecting surface and the included angle are 20m and 5°, respectively. The target is located at 125km away with an altitude of 6km for Fig. 5(a) and (b) and 7km for Fig. 5(c) and (d), respectively. The other parameter settings are the same as before. Fig. 5 presents the estimation

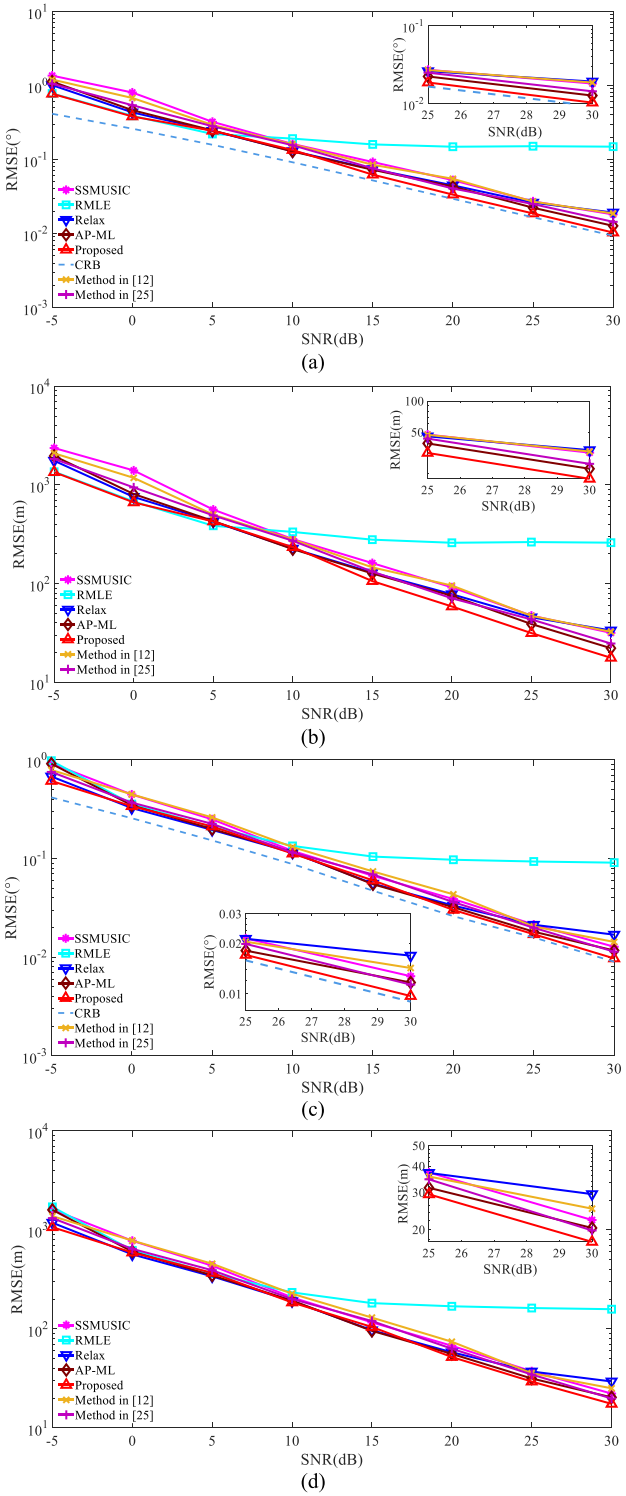

FIGURE 4. RMSE results of respective algorithms versus SNR using 32 snapshots with a horizontal reflecting surface. (a) target DOA estimation for h_t=4km; (b) target altitude estimation for h_t=4km; (c) target DOA estimation for h_t=5km; (d) target altitude estimation for h_t=5km. All results are averaged over 500 Monte Carlo trials.

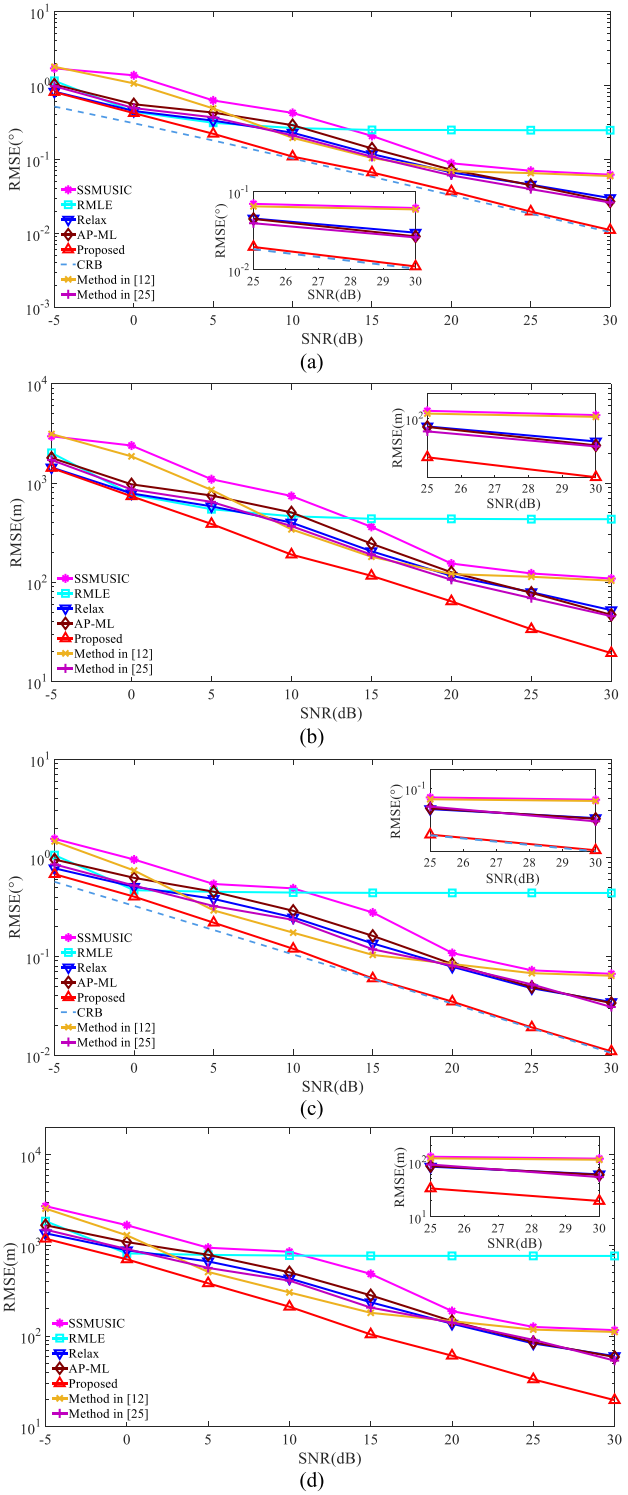

FIGURE 5. RMSEs results of respective algorithms versus SNR using 10 snapshots with a sloped reflecting surface. (a) target DOA estimation for h_t=6km; (b) target altitude estimation for h_t=6km; (c) target DOA estimation for h_t=7km; (d) target altitude estimation for h_t=7km. All results are averaged over 500 Monte Carlo trials.

performances of target direction and target altitude versus SNR, where the results are averaged over 500 independent trials.

It is observed from Fig. 5(a) – (d) that the performance of the RML algorithm is also heavily affected by the complex environment due to the same reason as that described

for the second experiment. We also observe that both the SSMUSIC algorithm and the method in [12] incur a considerable performance loss, possibly because the sample covariance matrix estimation is not precise enough to distinguish the direct path from the correlated multipath. Particularly, it is worth noting that the proposed algorithm presents a significant performance advantage over the other algorithms for the generalized scenario with a sloped reflecting surface and a small number of snapshots. Probably because the inherent structure information of the spatial signals is sufficiently exploited by taking the multipath attenuation coefficient into consideration in the proposed algorithm. This advantage makes our proposed algorithm attractive, especially for generalized scenario with complex terrain and/or a limited number of snapshots. The results in Fig. 5(a) and (c) also indicate that the proposed algorithm can approach the corresponding CRB in high SNR situation.

B. MEASURED DATA VALIDATION

In this subsection, real data is utilized and analyzed to test the target localization performance of the respective algorithms. The real data is measured by an experimental array radar system with twenty channels in elevation. The radar is located at a hilly terrain environment with a variety of ground surfaces such as vegetation, grove and cropland. The original measurement is processed by pulse compression, moving target indication and constant false alarm rate to detect targets and to form a trajectory. In particular, it is worth pointing out that only a few (e.g. ten or less) snapshots are available for most of the CPIs of the measured data. The flight path and the distance of the target relative to the radar are shown in Fig. 6 and Fig. 7, respectively. The processed results and estimation errors are given in Fig. 8 and Fig. 9, respectively. The dashed lines in

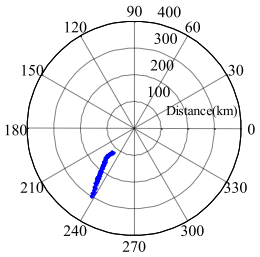

FIGURE 6. Navigational track map of the target.

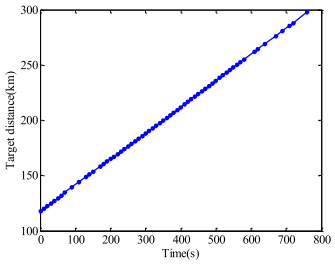

FIGURE 7. Varying target distance relative to the radar site.

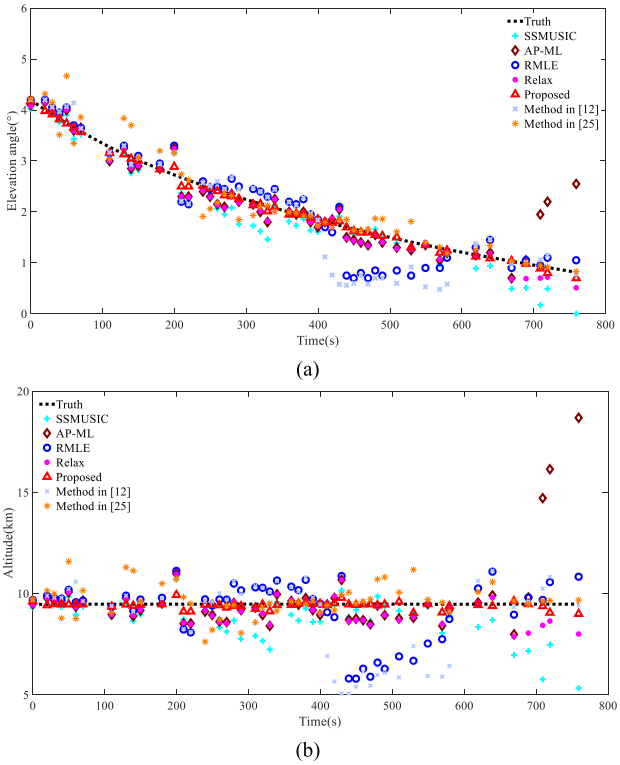

FIGURE 8. Processed results of the measured data by respective algorithms. (a) Comparison of elevation angles produced by SSMUSIC, AP-ML, RML, relax, subspace based method in [12], rank-1 based method in [25] and the proposed algorithms, (b) Comparison of altitudes produced by SSMUSIC, AP-ML, RML, relax, subspace based method in [12], rank-1 based method in [25] and the proposed algorithms.

Fig. 8 indicate the real target elevation angle or the real target altitude recorded by the global positioning system (GPS).

It can be observed that the performances of all the methods in Fig. 8 approach to the true elevation angle or altitude when the target elevation is larger than 2.5°, i.e., one half of a beamwidth. When the target elevation is less than 2.5°, however, the SSMUSIC algorithm, the RML algorithm and the method in [12] have large estimation fluctuations from the true values, which demonstrates that the real signal target and its multipath image cannot be accurately distinguished by these three methods in the complex terrain. It is worth mentioning that the method in [25] may have sometime considerable deviation, probably because the selection of the regularization parameter, which depends on the noise level in the received signal, is not appropriate. In other words, the robustness of the proposed algorithm is better than that of the method in [25]. In addition, the relax algorithm and the AP-ML algorithm are adversely affected by the complex scenario, especially in low elevation angle condition, whereas the proposed method is still capable of providing relatively accurate estimations of the target elevation angle and the target altitude. It is also seen from Fig. 9 that all the altitude errors estimated by the proposed algorithm are less than 260m, while the percentages of the estimated altitude error that is less than 260m are 35.29%, 49.02%, 39.22%, 47.06%, 37.29% and 56.86% for the SSMUSIC algorithm, the AP-ML algorithm,

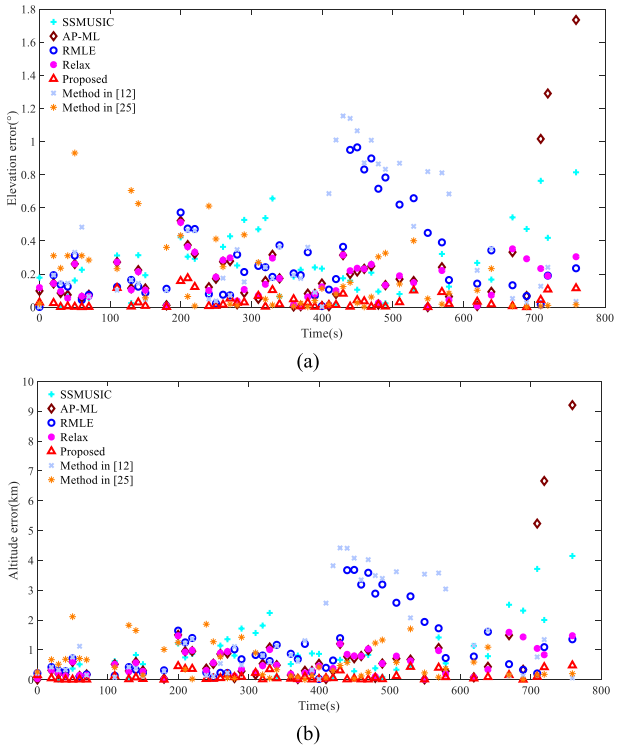

FIGURE 9. Estimation errors from the measured data by respective algorithms. (a) Errors of elevation angle produced by SSMUSIC, AP-ML, RML, relax, subspace based method in [12], rank-1 based method in [25] and the proposed algorithms (b) Errors of altitude produced by SSMUSIC, AP-ML, RML, relax, subspace based method in [12], rank-1 based method in [25] and the proposed algorithms.

the RML algorithm, the relax algorithm, the method in [12] and the method in [25], respectively. These measured data results demonstrate that the proposed algorithm is capable of locating a target under the complex terrain with a very limited number of measurements and without any prior knowledge of the reflected multipath.

V. CONCLUSIONS

This paper studied the problem of target localization in the presence of multipath propagation, where the influences caused by both multipaths from complex terrain environment and the limited number of available snapshots are taken into consideration. Considering the strong sparsity of the spatial signals, a tractable sparse representation based algorithm, combined with alternatingly iterative scheme and adaptive dictionary refinement technique, is proposed to deal with this problem. The algorithm started with a scheme of SVD to reduce both the signal dimension and the sensitivity to noise and to formulate a combination of multiple time sample sparse representation problem in the signal subspace domain. Then, a structural adaptive dictionary was introduced to exploit the inner structure information and to reduce the sparsity of the spatial signals. In addition, our proposed algorithm uses an efficient optimization procedure based on the combination of alternatingly iterative scheme and adaptive dictionary refinement technique, in which the target localization and the dictionary refinement are adaptively realized. Meanwhile, the CRB for the target's elevation angle was derived. Finally, the efficiency of the proposed algorithm was examined by various simulated scenarios and real measured data.

APPENDIX A

When there is no noise, (22) becomes

$$\begin{aligned}\mathbf{X} &= [\mathbf{x}(t_1), \cdots, \mathbf{x}(t_l), \cdots, \mathbf{x}(t_L)] \\ &= [\mathbf{B}_{\boldsymbol{\Omega}}\boldsymbol{\omega}(t_1), \cdots, \mathbf{B}_{\boldsymbol{\Omega}}\boldsymbol{\omega}(t_l), \cdots, \mathbf{B}_{\boldsymbol{\Omega}}\boldsymbol{\omega}(t_L)] \\ &= \mathbf{B}_{\boldsymbol{\Omega}}\mathbf{W}. \end{aligned} \tag{37}$$

We first consider the case of $L = 1$,

$$\mathbf{X} = \mathbf{x}(t_1) = \mathbf{B}_{\boldsymbol{\Omega}}\boldsymbol{\omega}(t_1). \tag{38}$$

It is clear that rank $(\mathbf{X}) = 1$.

Next, we focus on the case of $L > 1$. Since there is only one target, there is only one nonzero element in each column of $\mathbf{W}$, i.e., each $\boldsymbol{\omega}(t_l)$, where $l = 1, \cdots, L$, includes only one nonzero entry. Since it is assumed that the movement of a target can be neglected during the time interval $\{t_1, \cdots, t_L\}$, the indices of the nonzero entries of the columns in $\mathbf{W}$ should appear in the same row. This means that matrix $\mathbf{W}$ has only one non-zero row and all the other rows are zeros, i.e., the rank of matrix $\mathbf{W}$ is one. Thus, the rank of matrix $\mathbf{X}$ is one since $\mathbf{X}$ is not a zero matrix and its rank cannot be more than one.

APPENDIX B

In this appendix, we present the derivation of the Cramer-Rao bound for the target's elevation angle, where the multipath attenuation coefficient $\bar{\rho}$ is treated as an unknown parameter. Define $\boldsymbol{\psi} = [\mathbf{a}(\theta_d), \mathbf{a}(\theta_s)]$ and $\boldsymbol{\Gamma} = [1, \bar{\rho}]^T$, (7) can be equivalently expressed as

$$\mathbf{x}(t) = a\boldsymbol{\psi}\boldsymbol{\Gamma}s(t) + \mathbf{n}(t), \quad t \in \{t_1, \cdots, t_L\}. \tag{39}$$

The covariance matrix of the array measurement can be represented as

$$\begin{aligned}\mathbf{R}_x &= E\left\{\mathbf{x}(t)\mathbf{x}^H(t)\right\} \\ &= a^2\sigma_s^2\boldsymbol{\psi}\boldsymbol{\Gamma}\boldsymbol{\Gamma}^H\boldsymbol{\psi}^H + \sigma_N^2\mathbf{I}_M \end{aligned} \tag{40}$$

where $\sigma_s^2 = E\left\{s(t)s^H(t)\right\}$ is the signal power, and $\mathbf{I}_M$ is an $M \times M$ identity matrix.

Suppose there are L statistically independent samples during the observation time. Now, the logarithm of the joint probability density function can be expressed as

$$\begin{aligned}\ell &= \ln\{F[\mathbf{x}(t_1), \mathbf{x}(t_2), \cdots, \mathbf{x}(t_L)]\} \\ &= b - L\ln\{|\mathbf{R}_x|\} - \sum_{l=1}^{L}\mathbf{x}^H(t_l)\mathbf{R}_x^{-1}\mathbf{x}(t_l) \\ &= b - L\ln\{|\mathbf{R}_x|\} - Ltr\left\{\mathbf{R}_x^{-1}\hat{\mathbf{R}}_x\right\} \end{aligned} \tag{41}$$

where b is a constant term, and $\hat{\mathbf{R}}_x = \sum_{l=1}^{L} \mathbf{x}(t_l)\mathbf{x}^H(t_l)/L$. Let $\boldsymbol{\eta} = [\theta_d, \theta_s, \bar{\rho}_{\mathrm{Re}}, \bar{\rho}_{\mathrm{Im}}]$ as the unknown parameter vector, where $\bar{\rho}_{\mathrm{Re}}$ and $\bar{\rho}_{\mathrm{Im}}$ denote the real and imaginary parts of $\bar{\rho}$, respectively. Assume η_r represent the r-th element in $\boldsymbol{\eta}$. Thus, the (i,j)th element of the Fisher information matrix (FIM) can be expressed as

$$\mathbf{F}_{\eta_i\eta_j} = -E\left\{\frac{\partial^2 \ell}{\partial\eta_i\partial\eta_j}\right\}. \tag{42}$$

Since

$$\frac{\partial \mathbf{R}_x^{-1}}{\partial\eta_i} = -\mathbf{R}_x^{-1}\left(\frac{\partial \mathbf{R}_x}{\partial\eta_i}\right)\mathbf{R}_x^{-1}, \tag{43}$$

$$\frac{\partial \ln\left\{\left|\mathbf{R}_x^{-1}\right|\right\}}{\partial\eta_i} = tr\left\{\mathbf{R}_x^{-1}\left(\frac{\partial \mathbf{R}_x}{\partial\eta_i}\right)\right\}, \tag{44}$$

the first order derivative of ℓ with respect to η_i can be computed as

$$\begin{aligned}\frac{\partial \ell}{\partial\eta_i} &= -Ltr\left\{\mathbf{R}_x^{-1}\left(\frac{\partial \mathbf{R}_x}{\partial\eta_i}\right)\right\} + Ltr\left\{\mathbf{R}_x^{-1}\left(\frac{\partial \mathbf{R}_x}{\partial\eta_i}\right)\mathbf{R}_x^{-1}\hat{\mathbf{R}}_x\right\}\\ &= Ltr\left\{\mathbf{R}_x^{-1}\left(\frac{\partial \mathbf{R}_x}{\partial\eta_i}\right)\left(\mathbf{R}_x^{-1}\hat{\mathbf{R}}_x - \mathbf{I}\right)\right\}.\end{aligned} \tag{45}$$

The second order derivative can be similarly obtained as

$$\begin{aligned}\frac{\partial^2 \ell}{\partial\eta_i\partial\eta_j} &= Ltr\left\{\begin{array}{l}\dfrac{\partial\left(\mathbf{R}_x^{-1}\left(\partial\mathbf{R}_x/\partial\eta_i\right)\right)}{\partial\eta_j}\\ \times\left(\mathbf{R}_x^{-1}\hat{\mathbf{R}}_x - \mathbf{I}\right)\end{array}\right\}\\ &\quad + Ltr\left\{\begin{array}{l}\mathbf{R}_x^{-1}\left(\dfrac{\partial \mathbf{R}_x}{\partial\eta_i}\right)\\ \times\left(\dfrac{\partial\left(\mathbf{R}_x^{-1}\hat{\mathbf{R}}_x - \mathbf{I}\right)}{\partial\eta_j}\right)\end{array}\right\}\\ &= Ltr\left\{\begin{array}{l}\dfrac{\partial\left(\mathbf{R}_x^{-1}\left(\partial\mathbf{R}_x/\partial\eta_i\right)\right)}{\partial\eta_j}\\ \times\left(\mathbf{R}_x^{-1}\hat{\mathbf{R}}_x - \mathbf{I}\right)\end{array}\right\}\\ &\quad + Ltr\left\{\begin{array}{l}\mathbf{R}_x^{-1}\left(\dfrac{\partial \mathbf{R}_x}{\partial\eta_i}\right)\\ \times\left(\mathbf{R}_x^{-1}\dfrac{\partial(\mathbf{R}_x)}{\partial\eta_j}\mathbf{R}_x^{-1}\hat{\mathbf{R}}_x\right)\end{array}\right\}.\end{aligned} \tag{46}$$

By using (46), (42) can be further expressed as

$$\mathbf{F}_{\eta_i\eta_j} = Ltr\left\{\mathbf{R}_x^{-1}\frac{\partial \mathbf{R}_x}{\partial\eta_i}\mathbf{R}_x^{-1}\frac{\partial \mathbf{R}_x}{\partial\eta_j}\right\}. \tag{47}$$

Let $\dot{\mathbf{H}}_{\eta_i} = \partial\mathbf{H}/\partial\eta_i, \forall\, i$ and $\mathbf{H}$. Using (40), the derivative of $\mathbf{R}_x$ with respect to θ_i can be computed as

$$\frac{\partial \mathbf{R}_x}{\partial\theta_i} = \sigma_s^2\dot{\boldsymbol{\psi}}_{\theta_i}\boldsymbol{\Gamma}\boldsymbol{\Gamma}^H\boldsymbol{\psi}^H + \sigma_s^2\boldsymbol{\psi}\boldsymbol{\Gamma}\boldsymbol{\Gamma}^H\dot{\boldsymbol{\psi}}_{\theta_i}^H. \tag{48}$$

By utilizing the equation $tr\left\{\mathbf{R}_x + \mathbf{R}_x^H\right\} = 2\mathrm{Re}\left\{tr\left\{\mathbf{R}_x\right\}\right\}$, we obtain

$$\mathbf{F}_{\theta_i\theta_j} = 2L\sigma_s^4\mathrm{Re}\left\{tr\left(\begin{array}{l}\mathbf{R}_x^{-1}\dot{\boldsymbol{\psi}}_{\theta_i}\boldsymbol{\Gamma}\boldsymbol{\Gamma}^H\boldsymbol{\psi}^H\mathbf{R}_x^{-1}\dot{\boldsymbol{\psi}}_{\theta_j}\boldsymbol{\Gamma}\boldsymbol{\Gamma}^H\boldsymbol{\psi}^H\\ +\mathbf{R}_x^{-1}\boldsymbol{\psi}\boldsymbol{\Gamma}\boldsymbol{\Gamma}^H\dot{\boldsymbol{\psi}}_{\theta_i}^H\mathbf{R}_x^{-1}\dot{\boldsymbol{\psi}}_{\theta_j}\boldsymbol{\Gamma}\boldsymbol{\Gamma}^H\boldsymbol{\psi}^H\end{array}\right)\right\}. \tag{49}$$

Let $\dot{\boldsymbol{\psi}}_{\boldsymbol{\theta}} = \left[d\mathbf{a}(\theta_d)/d\theta_d, d\mathbf{a}(\theta_s)/d\theta_s\right]$, the FIM corresponding to $\boldsymbol{\theta} = [\theta_d, \theta_s]$ can be represented as

$$\begin{aligned}\mathbf{F}_{\boldsymbol{\theta}\boldsymbol{\theta}} &= 2L\sigma_s^4\mathrm{Re}\\ &\quad\times\left\{\begin{array}{l}\left(\boldsymbol{\Gamma}\boldsymbol{\Gamma}^H\boldsymbol{\psi}^H\mathbf{R}_x^{-1}\dot{\boldsymbol{\psi}}_{\boldsymbol{\theta}}\right)\odot\left(\boldsymbol{\Gamma}\boldsymbol{\Gamma}^H\boldsymbol{\psi}^H\mathbf{R}_x^{-1}\dot{\boldsymbol{\psi}}_{\boldsymbol{\theta}}\right)^T\\ +\left(\dot{\boldsymbol{\psi}}_{\boldsymbol{\theta}}^H\mathbf{R}_x^{-1}\dot{\boldsymbol{\psi}}_{\boldsymbol{\theta}}\right)\odot\left(\boldsymbol{\Gamma}\boldsymbol{\Gamma}^H\boldsymbol{\psi}^H\mathbf{R}_x^{-1}\boldsymbol{\psi}\boldsymbol{\Gamma}\boldsymbol{\Gamma}^H\right)^T\end{array}\right\}.\end{aligned} \tag{50}$$

Furthermore, the other elements of the FIM corresponding to the parameters in $\boldsymbol{\eta}$ can be similarly computed as follows

$$\begin{aligned}&\mathbf{F}_{\bar{\rho}_{\mathrm{Re}}\bar{\rho}_{\mathrm{Re}}}\\ &= Ltr\left\{\mathbf{R}_x^{-1}\left(\frac{\partial \mathbf{R}_x}{\partial\bar{\rho}_{\mathrm{Re}}}\right)\mathbf{R}_x^{-1}\left(\frac{\partial \mathbf{R}_x}{\partial\bar{\rho}_{\mathrm{Re}}}\right)\right\}\\ &= 2L\sigma_s^4\mathrm{Re}\\ &\quad\times\left\{\begin{array}{l}\left(\boldsymbol{\Gamma}^H\boldsymbol{\psi}^H\mathbf{R}_x^{-1}\boldsymbol{\psi}\dot{\boldsymbol{\Gamma}}_{\bar{\rho}_{\mathrm{Re}}}\right)\odot\left(\boldsymbol{\Gamma}^H\boldsymbol{\psi}^H\mathbf{R}_x^{-1}\boldsymbol{\psi}\dot{\boldsymbol{\Gamma}}_{\bar{\rho}_{\mathrm{Re}}}\right)^T\\ +\left(\dot{\boldsymbol{\Gamma}}_{\bar{\rho}_{\mathrm{Re}}}^H\boldsymbol{\psi}^H\mathbf{R}_x^{-1}\boldsymbol{\psi}\dot{\boldsymbol{\Gamma}}_{\bar{\rho}_{\mathrm{Re}}}\right)\odot\left(\boldsymbol{\Gamma}^H\boldsymbol{\psi}^H\mathbf{R}_x^{-1}\boldsymbol{\psi}\boldsymbol{\Gamma}\right)^T\end{array}\right\},\end{aligned} \tag{51}$$

$$\begin{aligned}&\mathbf{F}_{\bar{\rho}_{\mathrm{Im}}\bar{\rho}_{\mathrm{Im}}}\\ &= Ltr\left\{\mathbf{R}_x^{-1}\left(\frac{\partial \mathbf{R}_x}{\partial\bar{\rho}_{\mathrm{Im}}}\right)\mathbf{R}_x^{-1}\left(\frac{\partial \mathbf{R}_x}{\partial\bar{\rho}_{\mathrm{Im}}}\right)\right\}\\ &= 2L\sigma_s^4\mathrm{Re}\\ &\quad\times\left\{\begin{array}{l}\left(\boldsymbol{\Gamma}^H\boldsymbol{\psi}^H\mathbf{R}_x^{-1}\boldsymbol{\psi}\dot{\boldsymbol{\Gamma}}_{\bar{\rho}_{\mathrm{Im}}}\right)\odot\left(\boldsymbol{\Gamma}^H\boldsymbol{\psi}^H\mathbf{R}_x^{-1}\boldsymbol{\psi}\dot{\boldsymbol{\Gamma}}_{\bar{\rho}_{\mathrm{Im}}}\right)^T\\ +\left(\dot{\boldsymbol{\Gamma}}_{\bar{\rho}_{\mathrm{Im}}}^H\boldsymbol{\psi}^H\mathbf{R}_x^{-1}\boldsymbol{\psi}\dot{\boldsymbol{\Gamma}}_{\bar{\rho}_{\mathrm{Im}}}\right)\odot\left(\boldsymbol{\Gamma}^H\boldsymbol{\psi}^H\mathbf{R}_x^{-1}\boldsymbol{\psi}\boldsymbol{\Gamma}\right)^T\end{array}\right\},\end{aligned} \tag{52}$$

$$\begin{aligned}&\mathbf{F}_{\bar{\rho}_{\mathrm{Re}}\bar{\rho}_{\mathrm{Im}}}\\ &= Ltr\left\{\mathbf{R}_x^{-1}\left(\frac{\partial \mathbf{R}_x}{\partial\bar{\rho}_{\mathrm{Re}}}\right)\mathbf{R}_x^{-1}\left(\frac{\partial \mathbf{R}_x}{\partial\bar{\rho}_{\mathrm{Im}}}\right)\right\}\\ &= 2L\sigma_s^4\mathrm{Re}\\ &\quad\times\left\{\begin{array}{l}\left(\boldsymbol{\Gamma}^H\boldsymbol{\psi}^H\mathbf{R}_x^{-1}\boldsymbol{\psi}\dot{\boldsymbol{\Gamma}}_{\bar{\rho}_{\mathrm{Re}}}\right)\odot\left(\boldsymbol{\Gamma}^H\boldsymbol{\psi}^H\mathbf{R}_x^{-1}\boldsymbol{\psi}\dot{\boldsymbol{\Gamma}}_{\bar{\rho}_{\mathrm{Im}}}\right)^T\\ +\left(\dot{\boldsymbol{\Gamma}}_{\bar{\rho}_{\mathrm{Re}}}^H\boldsymbol{\psi}^H\mathbf{R}_x^{-1}\boldsymbol{\psi}\dot{\boldsymbol{\Gamma}}_{\bar{\rho}_{\mathrm{Re}}}\right)\odot\left(\boldsymbol{\Gamma}^H\boldsymbol{\psi}^H\mathbf{R}_x^{-1}\boldsymbol{\psi}\boldsymbol{\Gamma}\right)^T\end{array}\right\},\end{aligned} \tag{53}$$

$$\begin{aligned}&\mathbf{F}_{\bar{\rho}_{\mathrm{Re}}\boldsymbol{\theta}}\\ &= Ltr\left\{\mathbf{R}_x^{-1}\left(\frac{\partial \mathbf{R}_x}{\partial\bar{\rho}_{\mathrm{Re}}}\right)\mathbf{R}_x^{-1}\left(\frac{\partial \mathbf{R}_x}{\partial\boldsymbol{\theta}}\right)\right\}\\ &= 2L\sigma_s^4\mathrm{Re}\left\{\begin{array}{l}\left(\boldsymbol{\Gamma}^H\boldsymbol{\psi}^H\mathbf{R}_x^{-1}\dot{\boldsymbol{\psi}}_{\boldsymbol{\theta}}\right)\odot\left(\boldsymbol{\Gamma}\boldsymbol{\Gamma}^H\boldsymbol{\psi}^H\mathbf{R}_x^{-1}\boldsymbol{\psi}\dot{\boldsymbol{\Gamma}}_{\bar{\rho}_{\mathrm{Re}}}\right)^T\\ +\left(\dot{\boldsymbol{\Gamma}}_{\bar{\rho}_{\mathrm{Re}}}^H\boldsymbol{\psi}^H\mathbf{R}_x^{-1}\dot{\boldsymbol{\psi}}_{\boldsymbol{\theta}}\right)\odot\left(\boldsymbol{\Gamma}\boldsymbol{\Gamma}^H\boldsymbol{\psi}^H\mathbf{R}_x^{-1}\boldsymbol{\psi}\boldsymbol{\Gamma}\right)^T\end{array}\right\},\end{aligned} \tag{54}$$

$$\begin{aligned}&\mathbf{F}_{\bar{\rho}_{\mathrm{Im}}\boldsymbol{\theta}}\\ &= Ltr\left\{\mathbf{R}_x^{-1}\left(\frac{\partial \mathbf{R}_x}{\partial\bar{\rho}_{\mathrm{Im}}}\right)\mathbf{R}_x^{-1}\left(\frac{\partial \mathbf{R}_x}{\partial\boldsymbol{\theta}}\right)\right\}\\ &= 2L\sigma_s^4\mathrm{Re}\left\{\begin{array}{l}\left(\boldsymbol{\Gamma}^H\boldsymbol{\psi}^H\mathbf{R}_x^{-1}\dot{\boldsymbol{\psi}}_{\boldsymbol{\theta}}\right)\odot\left(\boldsymbol{\Gamma}\boldsymbol{\Gamma}^H\boldsymbol{\psi}^H\mathbf{R}_x^{-1}\boldsymbol{\psi}\dot{\boldsymbol{\Gamma}}_{\bar{\rho}_{\mathrm{Im}}}\right)^T\\ +\left(\dot{\boldsymbol{\Gamma}}_{\bar{\rho}_{\mathrm{Im}}}^H\boldsymbol{\psi}^H\mathbf{R}_x^{-1}\dot{\boldsymbol{\psi}}_{\boldsymbol{\theta}}\right)\odot\left(\boldsymbol{\Gamma}\boldsymbol{\Gamma}^H\boldsymbol{\psi}^H\mathbf{R}_x^{-1}\boldsymbol{\psi}\boldsymbol{\Gamma}\right)^T\end{array}\right\},\end{aligned} \tag{55}$$

$$\mathbf{F}_{\bar{\rho}_{\mathrm{Im}}\bar{\rho}_{\mathrm{Re}}} = \mathbf{F}_{\bar{\rho}_{\mathrm{Re}}\bar{\rho}_{\mathrm{Im}}}^H, \tag{56}$$

$$\mathbf{F}_{\boldsymbol{\theta}\bar{\rho}_{\mathrm{Re}}} = \mathbf{F}_{\bar{\rho}_{\mathrm{Re}}\boldsymbol{\theta}}^H, \tag{57}$$

$$\mathbf{F}_{\boldsymbol{\theta}\bar{\rho}_{\mathrm{Im}}} = \mathbf{F}_{\bar{\rho}_{\mathrm{Im}}\boldsymbol{\theta}}^H. \tag{58}$$

Now, the FIM matrix can be readily obtained by substituting (50)—(58) into (59), expressed as

$$\mathbf{F} = \begin{bmatrix} \mathbf{F}_{\boldsymbol{\theta}\boldsymbol{\theta}} & \mathbf{F}_{\boldsymbol{\theta}\bar{\rho}_{\mathrm{Re}}} & \mathbf{F}_{\boldsymbol{\theta}\bar{\rho}_{\mathrm{Im}}} \\ \mathbf{F}_{\bar{\rho}_{\mathrm{Re}}\boldsymbol{\theta}} & \mathbf{F}_{\bar{\rho}_{\mathrm{Re}}\bar{\rho}_{\mathrm{Re}}} & \mathbf{F}_{\bar{\rho}_{\mathrm{Re}}\bar{\rho}_{\mathrm{Im}}} \\ \mathbf{F}_{\bar{\rho}_{\mathrm{Im}}\boldsymbol{\theta}} & \mathbf{F}_{\boldsymbol{\theta}\bar{\rho}_{\mathrm{Im}}} & \mathbf{F}_{\bar{\rho}_{\mathrm{Im}}\bar{\rho}_{\mathrm{Im}}} \end{bmatrix}_{4\times 4}. \tag{59}$$

Then, it is easy to get the CRB of the target's elevation angle from the matrix $\mathbf{F}^{-1}$.

REFERENCES

[1] L. Lo and J. Litva, "Early results of multipath measurements on lake ontario (low angle radar tracking)," *IEEE Trans. Antennas Propag.*, vol. AP-34, no. 3, pp. 26–30, Mar. 1986.
[2] H. Xu, D. Wang, B. Ba, W. Cui, and Y. Zhang, "Direction-of-arrival estimation for both uncorrelated and coherent signals in coprime array," *IEEE Access*, vol. 7, pp. 18590–18600, 2019.
[3] H. Lan, Y. Liang, Q. Pan, F. Yang, and C. Guan, "An EM algorithm for multipath state estimation in OTHR target tracking," *IEEE Trans. Signal Process.*, vol. 62, no. 11, pp. 2814–2826, Jun. 2014.
[4] H. Y. Xu, Y. Zhang, B. Ba, D. Wang, and X. Li, "Fast Joint estimation of time of arrival and angle of arrival in complex multipath environment using OFDM," *IEEE Access*, vol. 6, pp. 60613–60621, 2018.
[5] R. O. Schmidt, "A signal subspace approach to multiple emitter location and spectral estimation," Ph.D. dissertation, Dept. Elect. Eng., Stanford Univ., Stanford, CA, USA, 1981.
[6] S. U. Pillai and B. H. Kwon, "Forward/backward spatial smoothing techniques for coherent signal identification," *IEEE Trans. Acoust., Speech Signal Process.*, vol. 37, no. 1, pp. 8–15, Jan. 1989.
[7] M. Shaghaghi and S. A. Vorobyov, "Subspace leakage analysis and improved DOA estimation with small sample size," *IEEE Trans. Signal Process.*, vol. 63, no. 12, pp. 3251–3265, Jun. 2015.
[8] A. L. Kintz and I. J. Gupta, "A modified MUSIC algorithm for direction of arrival estimation in the presence of antenna array manifold mismatch," *IEEE Trans. Antennas Propag.*, vol. 64, no. 11, pp. 4836–4847, Nov. 2016.
[9] D. H. Johnson and D. E. Dudgeon, *Array Signal Processing: Concepts and Techniques*. Englewood Cliffs, NJ, USA: Prentice-Hall, 1993.
[10] F. Khosravi, H. Moghadas, and P. Mousavi, "A GNSS antenna with a polarization selective surface for the mitigation of low-angle multipath interference," *IEEE Trans. Antennas Propag.*, vol. 63, no. 12, pp. 5287–5295, Dec. 2015.
[11] F. Yan, M. Jin, and X. Qiao, "Low-complexity DOA estimation based on compressed MUSIC and its performance analysis," *IEEE Trans. Signal Process.*, vol. 61, no. 8, pp. 1915–1930, Apr. 2013.
[12] Y. Liu, H. W. Liu, X.-G. Xia, L. Zhang, and B. Jiu, "Projection techniques for altitude estimation over complex multipath condition-based VHF radar," *IEEE J. Sel. Topics Appl. Earth Observ. Remote Sens.*, vol. 11, no. 7, pp. 2362–2375, Jul. 2018.
[13] Y. Liu, B. Jiu, H. Liu, L. Zhang, and Y. Zhao, "Compressive sensing for very high frequency radar with application to low-angle target tracking under multipath interference," in *Proc. 4th Int. Workshop Compressed Sens. Theory Appl. Radar, Sonar Remote Sens. (CoSeRa)*, Aachen, Germany, Sep. 2016, pp. 188–192.
[14] R. T. Suryaprakash and R. R. Nadakuditi, "Consistency and MSE performance of MUSIC-based DOA of a single source in white noise with randomly missing data," *IEEE Trans. Signal Process.*, vol. 63, no. 18, pp. 4756–4770, Sep. 2015.
[15] Z. H. Zhou, M. G. Christensen, J. R. Jensen, and H. C. So, "Joint DOA and fundamental frequency estimation based on relaxed iterative adaptive approach and optimal filtering," in *Proc. IEEE Int. Conf. Acoust., Speech Signal Process. (ICASSP)*, May 2013, pp. 6812–6816.
[16] M. Djeddou, A. Belouchrani, and S. Aouada, "Maximum likelihood angle-frequency estimation in partially known correlated noise for low-elevation targets," *IEEE Trans. Signal Process.*, vol. 53, no. 8, pp. 3057–3064, Aug. 2005.
[17] H. Krim and M. Viberg, "Two decades of array signal processing research: The parametric approach," *IEEE Signal Process. Mag.*, vol. 13, no. 4, pp. 67–94, Jul. 1996.
[18] P. Stoica and A. B. Gershman, "Maximum-likelihood DOA estimation by data-supported grid search," *IEEE Signal Process. Lett.*, vol. 6, no. 10, pp. 273–275, Oct. 1999.
[19] Y.-H. Choi, "Alternating projection for maximum-likelihood source localization using eigendecomposition," *IEEE Signal Process. Lett.*, vol. 6, no. 4, pp. 73–75, Apr. 1999.
[20] T. Lo and J. Litva, "Use of a highly deterministic multipath signal model in low-angle tracking," *IEE Proc. F-Radar Signal Process.*, vol. 138, no. 2, pp. 163–171, Apr. 1991.
[21] E. Bosse, R. M. Turner, and M. Lecours, "Tracking swerling fluctuating targets at low altitude over the sea," *IEEE Trans. Aerosp. Electron. Syst.*, vol. 27, no. 5, pp. 806–822, Sep. 1991.
[22] E. Bosse and R. M. Turner, "Height ambiguities in maximum likelihood estimation with a multipath propagation model," in *Proc. 22nd Asilomar Conf. Signals, Syst. Comput.*, Pacific Grove, CA, USA, Nov. 1988, pp. 690–695.
[23] A. Hizal and S. Koç, "Mitigating the multipath effects of low angle monopulse tracking by even difference pattern," in *Proc. 9th Eur. Radar Conf.*, Amsterdam, The Netherlands, Oct. 2012, pp. 290–293.
[24] D. B. Trizna, "A model for brewster angle damping and multipath effects on the microwave radar sea echo at low grazing angles," *IEEE Trans. Geosci. Remote Sens.*, vol. 35, no. 5, pp. 1232–1244, Sep. 1997.
[25] Y. Liu, B. Jiu, X.-G. Xia, H. Liu, and L. Zhang, "Height measurement of low-angle target using MIMO radar under multipath interference," *IEEE Trans. Aerosp. Electron. Syst.*, vol. 54, no. 2, pp. 808–818, Apr. 2018.
[26] M. L. Meeks, *Radar Propagation at Low Altitudes*. Dedham, MA, USA: Artech House, 1982.
[27] P. Beckmann and A. Spizzichino, *The Scattering of Electromagnetic Waves From Rough Surfaces*. Norwood, MA, USA: Artech House, 1987.
[28] L. Blake, *Radar Range-Performance Analysis*. Norwood, MA, USA: Artech House, 1986.
[29] R. Takahashi, K. Hirata, and H. Maniwa, "Altitude estimation of low elevation target over the sea for surface based phased array radar," in *Proc. IEEE Radar Conf.*, Arlington, VA, USA, May 2010, pp. 123–128.
[30] C. Beard, "Coherent and incoherent scattering of microwaves from the ocean," *IEEE Trans. Antennas Propag.*, vol. 9, no. 5, pp. 470–483, Sep. 1961.
[31] D. Y. Northam, "A stochastic simulation of low grazing angle, forward scatter, over-water multipath effects," Nav. Res. Lab., Washington, DC, USA, Tech. Rep. 5658, Dec. 1981.
[32] M.-A. Takizawa and M. Yukawa, "Efficient dictionary-refining kernel adaptive filter with fundamental insights," *IEEE Trans. Signal Process.*, vol. 64, no. 16, pp. 4337–4350, Aug. 2016.
[33] J. Fang, F. Wang, Y. Shen, H. Li, and R. S. Blum, "Super-resolution compressed sensing for line spectral estimation: An iterative reweighted approach," *IEEE Trans. Signal Process.*, vol. 64, no. 18, pp. 4649–4662, Sep. 2016.
[34] Y. C. Pati, R. Rezaifar, and P. S. Krishnaprasad, "Orthogonal matching pursuit: Recursive function approximation with applications to wavelet decomposition," presented at the 27th Asilomar Conf. Signals, Syst., Comput., Pacific Grove, CA, USA, Nov. 1993.
[35] J. A. Tropp and A. C. Gilbert, "Signal recovery from random measurements via orthogonal matching pursuit," *IEEE Trans. Inf. Theory*, vol. 53, no. 12, pp. 4655–4666, Dec. 2007.
[36] B. Mamandipoor, D. Ramasamy, and U. Madhow, "Newtonized orthogonal matching pursuit: Frequency estimation over the continuum," *IEEE Trans. Signal Process.*, vol. 64, no. 19, pp. 5066–5081, Oct. 2016.
[37] J. Zhu, L. Han, R. S. Blum, and Z. Xu, "Multi-snapshot Newtonized orthogonal matching pursuit for line spectrum estimation with multiple measurement vectors," *Signal Process.*, vol. 165, pp. 175–185, Dec. 2019.
[38] B. Mager, P. Lundrigan, and N. Patwari, "Fingerprint-based device-free localization performance in changing environments," *IEEE J. Sel. Areas Commun.*, vol. 33, no. 11, pp. 2429–2438, Nov. 2015.
[39] M. Alodeh, S. Chatzinotas, and B. Ottersten, "Constructive multiuser interference in symbol level precoding for the MISO downlink channel," *IEEE Trans. Signal Process.*, vol. 63, no. 9, pp. 2239–2252, May 2015.

YUAN LIU was born in Shaanxi, China, in 1989. He received the B.Eng. and Ph.D. degrees in electronic engineering from Xidian University, Xi'an, China, in 2012 and 2018, respectively.

He is currently working as a full-time Postdoctoral Research Fellow with the School of Electrical and Electronic Engineering, Nanyang Technological University, Singapore. His major research interests include multiple-input multiple-out radar, array signal processing, sparse signal recovery techniques, and their application in source localization.

HONGWEI LIU (M'04) received the M.S. and Ph.D. degrees, both in electronic engineering, from Xidian University, Xi'an, China, in 1995 and 1999, respectively, where he is currently a Professor with the National Laboratory of Radar Signal Processing. His research interests include radar automatic target recognition, radar signal processing, and adaptive signal processing.

XIANG-GEN XIA (M'97–S'00–F'09) received the B.S. degree in mathematics from Nanjing Normal University, Nanjing, China, the M.S. degree in mathematics from Nankai University, Tianjin, China, and the Ph.D. degree in electrical engineering from the University of Southern California, Los Angeles, CA, USA, in 1983, 1986, and 1992, respectively.

He was a Senior/Research Staff Member with Hughes Research Laboratories, Malibu, CA, USA, from 1995 to 1996. In September 1996, he joined the Department of Electrical and Computer Engineering, University of Delaware, Newark, DE, USA, where he is the Charles Black Evans Professor. His current research interests include space-time coding, MIMO and OFDM systems, digital signal processing, and SAR and ISAR imaging. He is the author of the book titled *Modulated Coding for Intersymbol Interference Channels* (New York, Marcel Dekker, 2000).

Dr. Xia received the National Science Foundation (NSF) Faculty Early Career Development (CAREER) Program Award, in 1997, the Office of Naval Research (ONR) Young Investigator Award, in 1998, and the Outstanding Overseas Young Investigator Award from the National Nature Science Foundation of China, in 2001. He is the Technical Program Chair of the Signal Processing Symposium, Globecom 2007 in Washington D.C., and the General Co-Chair of the International Conference on Acoustics, Speech and Signal Processing (ICASSP) 2005 in Philadelphia. He is currently serving and has served as an Associate Editor for numerous international journals, including the IEEE Wireless Communications Letters, the IEEE Transactions on Signal Processing, the IEEE Transactions on Wireless Communications, the IEEE Transactions on Mobile Computing, and the IEEE Transactions on Vehicular Technology.

LU WANG received the B.Eng. degree in electrical and electronic engineering from Xidian University, in 2007, the M.Eng. degree in signal processing from the National Lab of Radar Signal Processing, Xidian University, China, in 2010, and the Ph.D. degree from the School of Electrical and Electronic Engineering, Nanyang Technological University, Singapore, in 2014.

From 2015 to 2017, she was with the School of Marine Science and Technology, Northwestern Polytechnical University, Xi'an, China. She is currently with the School of Electronic and Electrical Engineering, Nanyang Technological University, Singapore. Her major research interests include sparse Bayesian learning, radar imaging (SAR/ISAR), and array signal processing.

GUOAN BI (SM'89) received the B.Sc. degree in radio communications from the Dalian University of Technology, Dalian, China, in 1982, and the M.Sc. degree in telecommunication systems and the Ph.D. degree in electronics systems from Essex University, Colchester, U.K., in 1985 and 1988, respectively. Since 1991, he has been with the School of Electrical and Electronic Engineering, Nanyang Technological University, Singapore. His research interests include DSP algorithms and hardware structures, and signal processing for various applications, including sonar, radar, and communications.